Precambrian Research xxx (xxxx) xxx–xxx

Contents lists available at ScienceDirect

Precambrian Research

journal homepage: www.elsevier.com/locate/precamres

Newly identified 1.89 Ga mafic dyke swarm in the Archean Yilgarn Craton, Western Australia suggests a connection with India

J. Camilla Stark[a,b,c,*], Xuan-Ce Wang[b,c], Steven W. Denyszyn[d], Zheng-Xiang Li[a,b,c], Birger Rasmussen[d], Jian-Wei Zi[b], Stephen Sheppard[b], Yebo Liu[a,b,c]

[a] Earth Dynamics Group, Curtin University, GPO Box U1987, Perth, WA 6845, Australia
[b] The Institute for Geoscience Research (TIGeR), Department of Applied Geology, Curtin University, GPO Box U1987, Perth, WA 6845, Australia
[c] Department of Applied Geology, Curtin University, GPO Box U1987, Perth, WA 6845, Australia
[d] School of Earth Sciences, University of Western Australia, Perth, WA 6009, Australia

ARTICLE INFO

Keywords:
Yilgarn Craton
Mafic dykes
Geochronology
U-Pb baddeleyite
Large Igneous Province
Boonadgin dykes

ABSTRACT

The Archean Yilgarn Craton in Western Australia is intruded by numerous mafic dykes of varying orientations, which are poorly exposed but discernible in aeromagnetic maps. Previous studies have identified two craton-wide dyke swarms, the 2408 Ma Widgiemooltha and the 1210 Ma Marnda Moorn Large Igneous Provinces (LIP), as well as limited occurrences of the 1075 Ma Warakurna LIP in the northern part of the craton. We report here a newly identified NW-trending mafic dyke swarm in southwestern Yilgarn Craton dated at 1888 ± 9 Ma with ID-TIMS U-Pb method on baddeleyite from a single dyke and at 1858 ± 54 Ma, 1881 ± 37 and 1911 ± 42 Ma with *in situ* SHRIMP U-Pb on baddeleyite from three dykes. Preliminary interpretation of aeromagnetic data indicates that the dykes form a linear swarm several hundred kilometers long, truncated by the Darling Fault in the west. This newly named Boonadgin dyke swarm is synchronous with post-orogenic extension and deposition of granular iron formations in the Earaheedy basin in the Capricorn Orogen and its emplacement may be associated with far field stresses. Emplacement of the dykes may also be related to initial stages of rifting and formation of the intracratonic Barren Basin in the Albany-Fraser Orogen, where the regional extensional setting prevailed for the following 300 million years. Recent studies and new paleomagnetic evidence raise the possibility that the dykes could be part of the coeval 1890 Ma Bastar-Cuddapah LIP in India. Globally, the Boonadgin dyke swarm is synchronous with a major orogenic episode and records of intracratonic mafic magmatism on many other Precambrian cratons.

1. Introduction

Regardless of their proposed mechanism of formation (e.g., mantle plume, flux melting, passive rifting or global mantle warming), large igneous provinces (LIPs; Coffin and Eldholm, 1994), including mafic dyke swarms, appear to be intimately connected with deep-Earth dynamics and supercontinent cycles (e.g., Condie, 2004; Prokoph et al., 2004; Bleeker and Ernst, 2006; Ernst et al., 2008; Li and Zhong, 2009; Goldberg, 2010). Mafic dyke swarms act as important markers for supercontinent reconstructions (e.g., Ernst and Buchan, 1997; Buchan et al., 2001; Bleeker and Ernst, 2006; Ernst and Srivastava, 2008; Ernst et al., 2010, 2013) and as indicators of paleostress fields and pre-existing crustal weaknesses (Ernst et al., 1995; Hoek and Seitz, 1995; Halls and Zhang, 1998; Hou, 2012; Ju et al., 2013). Key to such application is the availability of high-precision geochronology for mafic dykes. Recent studies have shown that orientation alone cannot be reliably used to distinguish between different dyke generations, especially near major tectonic boundaries and craton scale structures such as continental rifts (e.g., Hanson et al., 2004; Wingate, 2007; French and Heaman, 2010; Belica et al., 2014).

Like many other Archean cratons worldwide, the Yilgarn Craton in Western Australia is intruded by many generations of dyke suites with different orientations. Currently, robust geochronology is only available for two craton-wide dyke swarms at 2408 Ma (Sofoulis, 1965; Evans, 1968; Hallberg, 1987; Doehler and Heaman, 1998; Nemchin and Pidgeon, 1998; Wingate, 1999; French et al., 2002) and at 1210 Ma (Marnda Moorn LIP; Wingate et al., 1998, 2000; Wingate, 2007), and for limited dyke occurrences at 1075 Ma (Warakurna LIP; Wingate et al., 2002, 2004) and ca. 735 Ma (Nindibillup dykes; Spaggiari et al., 2009, 2011; Wingate, 2017). The magmatic record ("barcode") for the Yilgarn Craton dyke swarms is very limited compared with other Archean cratons, such as the Superior and Kola-Karelia Cratons (Ernst and

* Corresponding author at: Earth Dynamics Group, Curtin University, GPO Box U1987, Perth, WA 6845, Australia.
E-mail address: c.stark@postgrad.curtin.edu.au (J.C. Stark).

https://doi.org/10.1016/j.precamres.2017.12.036
Received 23 September 2017; Accepted 17 December 2017

Bleeker, 2010; Ernst et al., 2010). The apparent absence of mafic magmatism in the Yilgarn Craton during the major global episode of juvenile magmatism and crustal growth at ca. 1890 Ma is surprising since this event is found on most other Precambrian cratons worldwide (Heaman et al., 1986, 2009; Hanson et al., 2004; French et al., 2008; Minifie et al., 2008; Buchan et al., 2010; Ernst and Bell, 2010; Söderlund et al., 2010). The lack of geochronology and paleomagnetic data from the Yilgarn Craton between ca. 1900 Ma and 1300 Ma, the proposed time interval for the supercontinent Nuna/Columbia, is especially problematic for paleographic reconstructions.

Here we report *in situ* SHRIMP and ID-TIMS U-Pb results for a previously unidentified NW-trending Paleoproterozoic mafic dyke suite in the southwestern Yilgarn Craton and discuss the tectonic setting during its emplacement. A direct record of Paleoproterozoic tectonic events in the craton margins is largely absent due to extensive overprinting by younger events, so we also evaluate evidence from remnant Proterozoic sedimentary basins, which preserve a history of past tectonic setting, crustal architecture and lithospheric stress fields. In light of previous studies suggesting India-Yilgarn connection (Mohanty, 2012, 2015) and recent paleomagnetic data (Belica et al., 2014; Liu et al., 2016, 2017) we consider the possibility that the dykes may be associated with the coeval Bastar-Cuddapah LIP in India.

2. Regional geology

The Yilgarn Craton is a ca. 900 × 1000 km Archean crustal block comprising six accreted terranes: the Southwest, Narryer, Youanmi, Kalgoorlie, Kurnalpi and Burtville terranes, the latter three forming the Eastern Goldfields Superterrane (Fig. 1). These comprise variably metamorphosed granites and volcanic and sedimentary rocks with protolith ages between ca. 3730 and 2620 Ma (Cassidy et al., 2005, 2006 and references therein) and are thought to represent a series of volcanic arcs, back arc basins and microcontinents, which amalgamated between ca. 2900 and 2700 Ma (Myers, 1993; Wilde et al., 1996). Abundant granites were emplaced between ca. 2760 Ma and 2630 Ma (Cassidy et al., 2006 and references therein) and the entire craton underwent intense metamorphism and hydrothermal activity between 2780 and 2630 Ma (Myers, 1993; Nemchin et al., 1994; Nelson et al., 1995; Wilde et al., 1996). The Southwest Terrane comprises multiply deformed ca. 3200–2800 Ma high-grade metasedimentary rocks and ca. 2720–2670 Ma meta-igneous rocks intruded by 2750–2620 Ma granites (Myers, 1993; Wilde et al., 1996; Nemchin and Pidgeon, 1997).

The Yilgarn Craton is bounded by three Proterozoic orogenic belts: the ca. 2005–570 Ma Capricorn Orogen in the north (Cawood and Tyler, 2004a; Sheppard et al., 2010a; Johnson et al., 2011), the ca. 1815–1140 Ma Albany-Fraser Orogen in the south and east (Nelson et al., 1995; Clark et al., 2000; Spaggiari et al., 2015), and the ca. 1090–525 Ma Pinjarra Orogen in the west (Myers, 1990; Wilde, 1999; Ksienzyk et al., 2012). Prolonged lateritic weathering has produced the modern denuded landscape and poor exposure of basement rocks (Anand and Paine, 2002).

Following cratonisation toward the end of the Archean, the Yilgarn Craton collided along the Capricorn Orogen with the combined Pilbara Craton-Glenburgh Terrane by 1950 Ma to form the West Australian Craton (WAC: Sheppard et al., 2004, 2010a, b; Johnson et al., 2011). Four syn- to post-orogenic sedimentary basins developed along the southern Capricorn Orogen, including the Earaheedy Basin in the east (Pirajno et al., 2009). The Earaheedy succession was thought to be post-1800 Ma in age, but new dating (Rasmussen et al., 2012; Sheppard et al., 2016) shows that the basin comprises three unconformity-bound packages at ca. 1990–1950 Ma, ca. 1890 Ma and ca. 1890–1810 Ma.

The Yilgarn Craton is intruded by a large number of dykes of

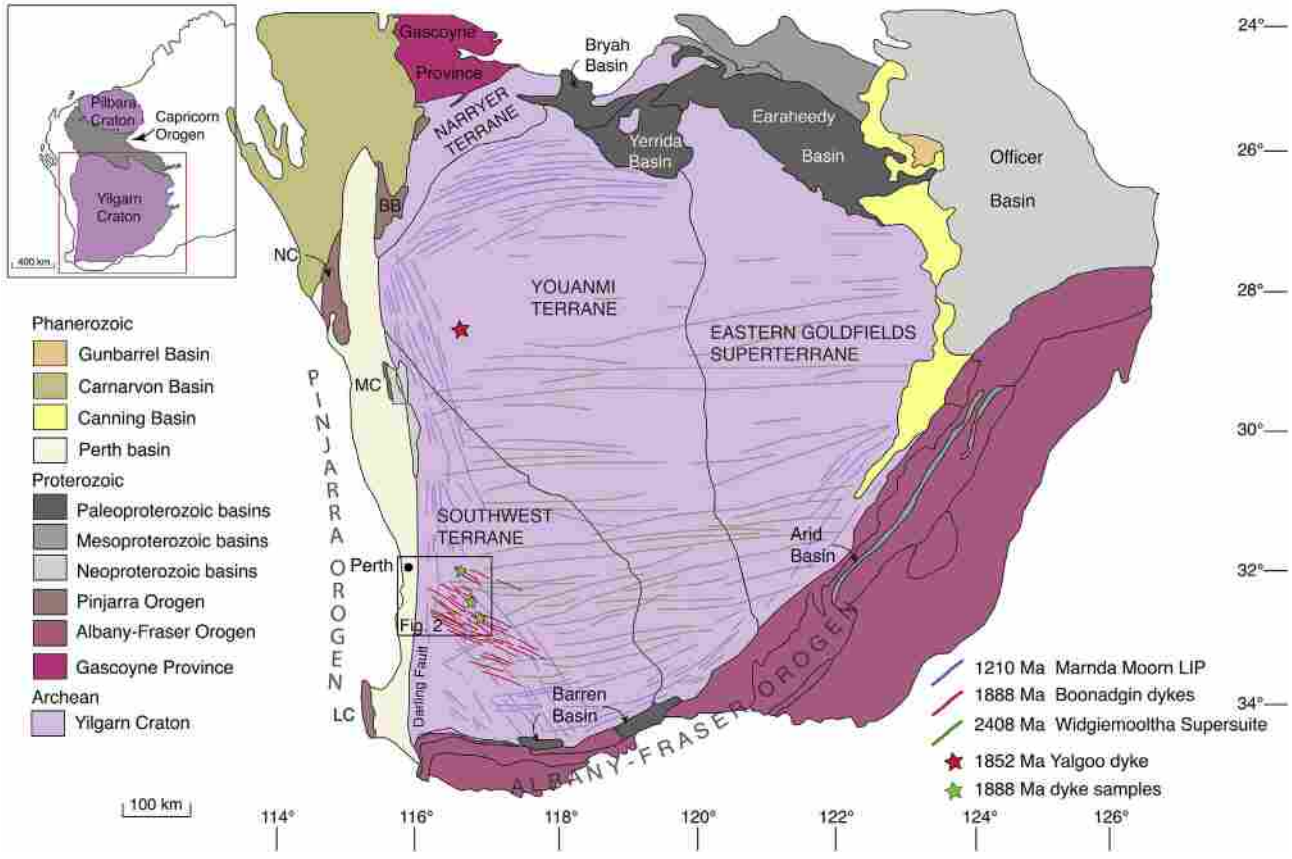

Fig. 1. Map of the Yilgarn showing major tectonic units and the Capricorn and Albany-Fraser Orogens. Inset shows the extent of the West Australian Craton (Pilbara Craton, Yilgarn Craton and Capricorn Orogen). From Geological Survey of Western Australia 1:2.5M Interpreted Bedrock Geology 2015 and 1:10M Tectonic Units 2016.

different orientations with the dyke density increasing towards the southern and western craton margins (Hallberg, 1987; Tucker and Boyd, 1987). The dykes are discernible in aeromagnetic data but difficult to sample due to deep weathering and thick regolith cover. The oldest known dykes belong to the E-W to NE-SW trending 2408 Ma Widgiemooltha Supersuite (Sofoulis, 1965; Evans, 1968; Campbell et al., 1970; Hallberg, 1987; Doehler and Heaman, 1998; Nemchin and Pidgeon, 1998; Wingate, 1999, 2007; French et al., 2002). The Widgiemooltha dykes are up to 3.2 km wide and extend up to 700 km across the craton, with the largest intrusions (Jimberlana and Binneringie) showing well developed igneous layering (Campbell et al., 1970; Lewis, 1994). The dykes exhibit dual magnetic polarity (Tucker and Boyd, 1987; Boyd and Tucker, 1990) and recent geochronology and paleomagnetic data suggest that their emplacement may have involved several pulses (Wingate, 2007; Pisarevsky et al., 2015). The second craton-wide suite is the 1210 Ma Marnda Moorn LIP which consists of several sub-swarms of different orientations intruding along the craton margins (Isles and Cooke, 1990; Evans, 1999; Wingate et al., 2000; Pidgeon and Nemchin, 2001; Pidgeon and Cook, 2003; Wingate and Pidgeon, 2005; Wingate, 2007; Claoué-Long and Hoatson, 2009). Outcrops in the southeast are limited to a single occurrence, and the extent of the dykes in the northeast is unknown due to cover rocks but one E-W oriented dioritic dyke dated at 1215 ± 11 Ma has been reported further inland (Qiu et al., 1999). Other identified dyke swarms with limited occurrences include the SW-trending dykes of the 1075 Ma Warakurna LIP in the northern Yilgarn Craton (Wingate et al., 2004), the WNW-trending ca. 735 Ma Nindibillup dykes in the central and SE Yilgarn Craton (Spaggiari et al., 2009, 2011; Wingate, 2017) and the undated (likely < 1140 Ma) NW-trending Beenong dykes in the SE Yilgarn Craton (Wingate, 2007; Spaggiari et al., 2009, 2011).

3. Samples

3.1. Field sampling

Field sampling sites were targeted using satellite imagery (Landsat/Copernicus or Astrium/CNES from Google Earth), aeromagnetic data (20–40 m cell size, Geoscience Australia magnetic grid of Australia V6 2015 base reference) and 1:250,000 geological maps from the Geological Survey of Western Australia.

Four block samples were collected from outcrops within agriculturally cleared areas where the dykes stand out as small ridges. Sample WDS09 was collected from an outcrop ca. 18 km southwest of the town of Pingelly, sample 16WDS01 and 16WDS02 ca. 29 km northwest of Pingelly and sample 16WDS06 ca. 14 km southwest of the village of Gwambygine (Fig. 2). Coordinates for sample locations are given in Table 1. Basement rocks are only exposed at the WDS09 outcrop where the dyke intrudes Archean migmatitic gneiss with a sharp chilled margin. At the 16WDS01/16WDS02 and 16WDS06 sites, geological mapping indicates that the country rocks to the dykes are mainly Archean granites. The outcrops are fresh with weathering forming a thin crust best visible along fractures.

3.2. Sample description

All samples are dolerites with intergranular ophitic to sub-ophitic texture, comprising ca. 50% plagioclase, 45% clinopyroxene, 1–2% quartz, 2–3% opaque minerals (ilmenite, magnetite and minor pyrite) and trace biotite and apatite. Sample WDS09 is relatively fresh but samples 16WDS01/02 and 16WDS06 in the northern part of the sampling area are more altered, with most clinopyroxene grains partially altered to chlorite and green amphibole. Plagioclase is affected by sericitisation but most grains still show twinning. Biotite is associated with the opaque minerals, forming corona like rims. The main U- and Th-bearing accessory minerals are baddeleyite and zirconolite, only identifiable under SEM due to their small size, typically ≤70 μm long and 20–30 μm across. Some crystals show thin zircon rims or alteration to zircon along fractures but most appear pristine.

4. U-Pb geochronology and geochemistry

4.1. SHRIMP U-Pb geochronology

Polished thin sections were scanned to identify baddeleyite, zircon and zirconolite with a Hitachi TM3030 scanning electron microscope (SEM) equipped with energy dispersive X-ray spectrometer (EDX) at Curtin University. For SHRIMP U-Pb dating, selected grains were drilled directly from the thin sections using a micro drill and mounted into epoxy disks, which were cleaned and coated with 40 nm of gold. Baddeleyite forms unaltered subhedral to euhedral equant and tabular grains and laths, some with thin zircon rims, and most are < 60 μm long and up to 20–30 μm across (Fig. 3).

Baddeleyite was analysed for U, Th and Pb using the sensitive high-resolution ion microprobe (SHRIMP II) at the John de Laeter Centre at Curtin University in Perth, Australia, following standard operating procedures after Compston et al. (1984). The SHRIMP analysis method for mounts with polished thin section plugs outlined in Rasmussen and Fletcher (2010) was modified for baddeleyite (SHRIMP operating parameters in Table 2). During each analysis session, standard zircon OG1 (Stern et al., 2009) was used to monitor instrumental mass fractionation and BR266 zircon (Stern, 2001) was used for calibrating U and Th concentration and as an accuracy standard. Phalaborwa baddeleyite (Heaman, 2009) was employed as an additional accuracy standard. Typical spot size with primary O_2^- current was 10–15 μm at 0.8–1.4 nA. Data were processed with Squid version 2.50 (Ludwig, 2009) and Isoplot version 3.76.12 (Ludwig, 2012). For common Pb correction, 1890 Ma common Pb isotopic compositions were calculated from the Stacey and Kramers (1975) two-stage terrestrial Pb isotopic evolution model. Analyses with > 1% common Pb (in ^{206}Pb) or > 10% discordance (see footnote in Table 3 for definition) are considered unreliable and were disregarded in age calculations. The assigned 1σ external Pb/U error for all analyses is 1%, except for 1.04% for 16WDS06. All weighted mean ages are given at 95% confidence level, whereas individual analyses are presented with 1σ error.

4.2. ID-TIMS U-Pb geochronology

A sample for ID-TIMS U-Pb geochronology was selected based on results from the SHRIMP dating and the highest number of identified baddeleyites in thin section. A block sample was first sawn from the field sample to remove weathering, then crushed, powdered and processed using a mineral-separation technique amended from Söderlund and Johansson (2002). Baddeleyite grains were handpicked under ethanol under a stereographic optical microscope and selected grains were cleaned with concentrated distilled HNO_3 and HCl. Due to the small size of the grains, no chemical separation methods were required.

Samples were spiked with a University of Western Australia in-house ^{205}Pb-^{235}U tracer solution, which has been calibrated against SRM981, SRM982 (for Pb), and CRM 115 (for U), as well as an externally-calibrated U-Pb solution (the JMM solution from the EarthTime consortium). This tracer is regularly checked using “synthetic zircon” solutions that yield U-Pb ages of 500 Ma and 2000 Ma, provided by D. Condon (BGS). Dissolution and equilibration of spiked single crystals was by vapour transfer of HF, using Teflon microcapsules in a Parr pressure vessel placed in a 200 °C oven for six days. The resulting residue was re-dissolved in HCl and H_3PO_4 and placed on an outgassed, zone-refined rhenium single filament with 5 μL of silicic acid gel. U–Pb isotope analyses were carried out using a Thermo Triton T1 mass spectrometer, in peak-jumping mode using a secondary electron multiplier. Uranium was measured as an oxide (UO_2). Fractionation and deadtime were monitored using SRM981 and SRM 982. Mass fractionation was 0.02 ± 0.07%/amu. Data were reduced and plotted using

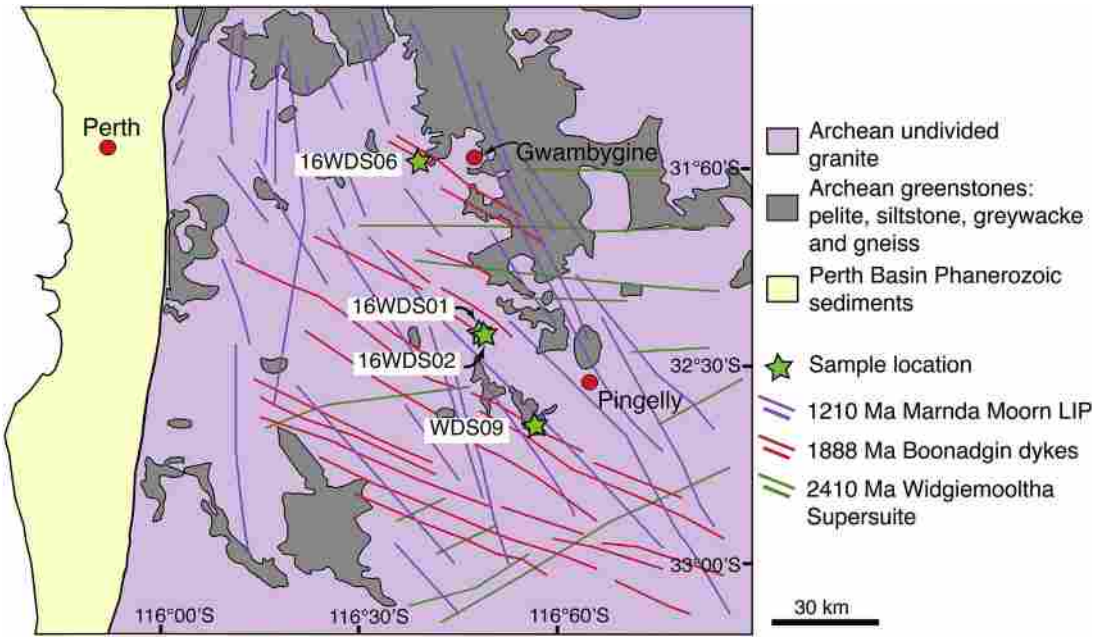

Fig. 2. Sampling locations. See Table 1 for detailed information.

Table 1
Sample locations.

Dyke ID	Dlat/Dlon	Samples	Comments
WDS09	32 39.339S 116 57.132E	WDS09M-N, WDS09RSA-B	NW trending dolerite dyke near West Pingelly
16WDS01	32 24.738S 116 48.818E	16WDS01A-D	NNW trending dolerite dyke west of Brookton, ridge
16WDS02	32 24.740S 116 48.798E	16WDS02A-D	NNW trending dolerite dyke west of Brookton. Same dyke as 16WDS01
16WDS06	31 59.973S 116 39.699E	16WDS06A-D	NW trending dyke near Talbot

Notes: Datum WGS84, Dlat = decimal latitude, Dlon = decimal longitude.

the software packages Tripoli (from CIRDLES.org) and Isoplot 4.15 (Ludwig, 2011). All uncertainties are reported at 2σ. U decay constants are from Jaffey et al. (1971). The weights of the baddeleyite crystals were calculated from measurements of photomicrographs and estimates of the third dimension. The weights are used to determine U and Pb concentrations and do not contribute to the age calculation. An uncertainty of ± 50% may be attributed to the concentration estimate.

4.3. Geochemistry

Slabs were sawn from block samples to remove weathering. After an initial crush, a small fraction of material was separated and chips with fresh fracture surfaces were handpicked under the microscope and pulverised in an agate mill for isotope analysis. Remaining material was pulverised in a low-Cr steel mill for major and trace element analysis.

Major element analysis was undertaken at Intertek Genalysis Laboratories in Perth, Western Australia using X-ray fluorescence (XRF) using the Geological Survey of Western Australia (GSWA) standard BB1 (Morris, 2007) and Genalysis laboratory internal standards SARM1 and SY-4. Trace element analysis was carried out at University of Queensland (UQ) on a Thermo XSeries 2 inductively coupled plasma mass spectrometer (ICP-MS) equipped with an ESI SC-4 DX FAST autosampler, following procedure for ICP-MS trace element analysis by Eggins et al. (1997) modified by the UQ Radiogenic Isotope Laboratory (Kamber et al., 2003). Sample solutions were diluted 4000 times and 12 ppb ^{6}Li, 6 ppb ^{61}Ni, Rh, In and Re, and 4.5 ppb ^{235}U internal spikes were added. USGS W2 was used as reference standard and crossed checked with BIR-1, BHVO-2 or other reference materials. All major element analyses have precision better than 5% and all trace element analyses have relative standard deviation (RSD) < 2%.

Rb-Sr and Sm-Nd isotope analyses were carried out at the University of Melbourne (e.g., Maas et al., 2005, 2015). Small splits (70 mg) of rock powders were spiked with ^{149}Sm-^{150}Nd and ^{85}Rb-^{84}Sr tracers, followed by dissolution at high pressure in an oven, using Krogh-type PTFE vessels with steel jackets. Sm, Nd and Sr were extracted using EICHROM Sr-, TRU- and LN-resin, and Rb was extracted using cation exchange (AG50-X8, 200–400 mesh resin). Isotopic analyses were carried out on a NU Plasma multi-collector ICP-MS coupled to a CETAC Aridus desolvation system operated in low-uptake mode. Raw data for spiked Sr and Nd fractions were corrected for instrumental mass bias by normalizing to ^{88}Sr/^{86}Sr = 8.37521 and ^{146}Nd/^{145}Nd = 2.0719425 (equivalent to ^{146}Nd/^{144}Nd = 0.7219), respectively, using the exponential law as part of an on-line iterative spike-stripping/internal normalization procedure. Sr and Nd isotope data are reported relative to SRM987 = 0.710230 and La Jolla Nd = 0.511860 and have typical in-run precisions (2sd) of ± 0.000020 (Sr) and ± 0.000012 (Nd). External precision (reproducibility, 2sd) is ± 0.000040 (Sr) and ± 0.000020 (Nd). External precisions for ^{87}Rb/^{86}Sr and ^{147}Sm/^{144}Nd obtained by isotope dilution are ± 0.5% and ± 0.2%, respectively.

5. Results

5.1. SHRIMP U-Pb geochronology

Seventeen analyses were obtained from thirteen baddeleyite grains (nine grains from WDS09, one grain from 16WDS01 and three grains from

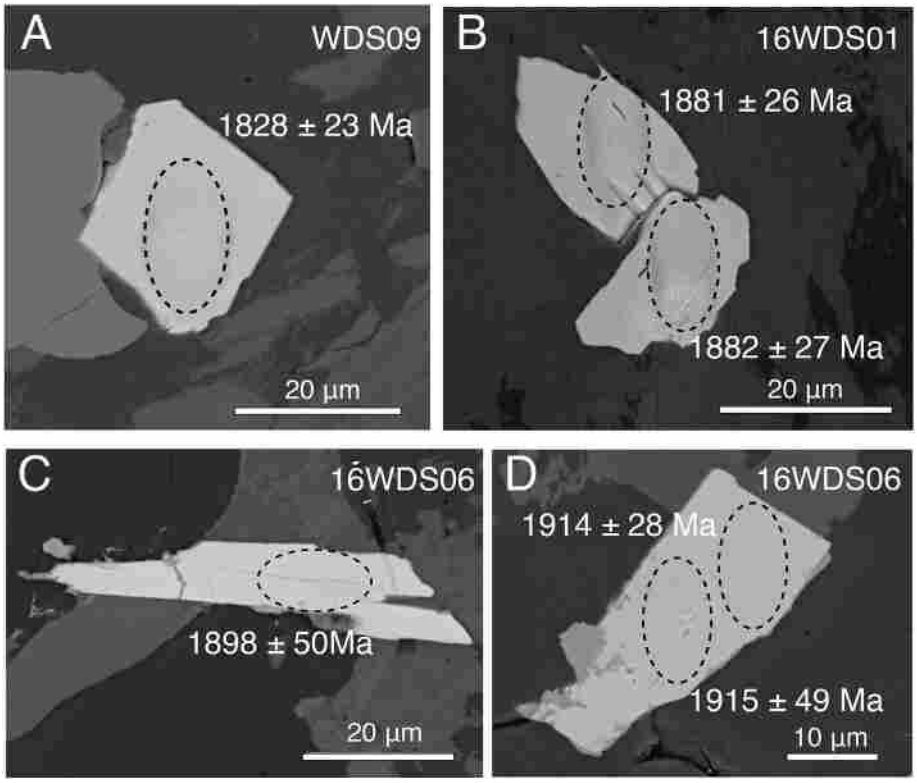

Fig. 3. SEM backscatter images showing SHRIMP baddeleyite spots and dates. (A) WDS09-2B (B) 16WDS01-372B (C) 16WDS06-405B (D) 16WDS06-406B.

Table 2
SHRIMP operating parameters.

Mount	CS16-1	CS16-6	CS16-7
Dykes analysed	WDS09, WDS09RS	16WDS01	16WDS06
Date analysed	21-Jul-16	14-Sep-16	6-Sep-16
Kohler aperture (µm)	50	50	50
Spot size (micrometres)	11	9	7
O_2^- primary current (nA)	0.9	0.6	0.2
Number of scans per analysis	8	8	8
Total number of analyses	23	32	34
Number of standard analyses	13	13	14
Pb/U external precision% (1σ)	1.00	1.00	1.00
Raster time (seconds)	120	180	180
Raster aperture (µm)	90	90	80

Notes: 1) Mass resolution for all analyses ≥5000 at 1% peak height; 2) BR266, OGC, Phalaborwa and NIST used as standards for each session; 3) Count times for each scan: ^{204}Pb, ^{206}Pb, ^{208}Pb = 10 s, ^{207}Pb = 30 s.

16WDS06) during three SHRIMP sessions (Fig. 4; detailed U-Pb data are given in Table 3). The analysed baddeleyites have low to moderate U concentrations varying from 47 to 449 ppm (median = 181 ppm) and low Th from 5 to 76 ppm, with Th/U ratios ranging from 0.02 to 0.47. Eight analyses were excluded based on their high common Pb (> 1% ^{206}Pb) and/or > 10% discordance. Sample WDS09 yielded a common Pb-corrected weighted mean ^{207}Pb/^{206}Pb date of 1858 ± 54 Ma (MSWD = 1.80, 4 analyses from 4 grains). If spot WDS09N5.29B-1, which is near-concordant (6% discordance) but contains slightly higher common Pb (1.45%) is included, the weighted mean is 1860 ± 41 Ma (MSWD = 1.4, n = 5). Two analyses on a single grain from 16WDS01 yield a ^{207}Pb/^{206}Pb weighted mean of 1881 ± 37 Ma (MSWD = 0.00075) and three analyses on 2 grains from 16WDS06 give a weighted mean of 1911 ± 42 Ma. Collectively, the 9 analyses on five baddeleyite grains from three samples give ^{207}Pb/^{206}Pb dates overlapping with each other within uncertainties; combining them yields a weighted mean of 1874 ± 25 Ma (MSWD = 1.3), which is interpreted as the best approximation of the crystallisation age of the dykes.

5.2. ID-TIMS U-Pb geochronology

Four baddeleyite crystals were analysed from sample WDS09 (Table 4, Fig. 5). Calculated weights are on the order of 0.1 µg, with low calculated U concentrations, all below 50 ppm. One grain has an apparently very low U content (3 ppm) and a concomitant low ^{206}Pb/^{204}Pb ratio of 30. This results in a relatively imprecise age determination and large analytical uncertainties for all data are the result of very low radiogenic Pb concentrations. Calculated U concentrations are unusually low for baddeleyite; this may reflect an overestimate of the grain weights, but the low Pb abundance (both radiogenic and common Pb) also implies a low initial U concentration. Th/U ratios are < 0.1, a typical value for baddeleyite. One datum is discordant but the coherence in ^{207}Pb/^{206}Pb age for all baddeleyite crystals supports our interpretation of the analyses representing a single magmatic crystallization age. The weighted-mean ^{207}Pb/^{206}Pb dates of the four single-crystal analyses is 1863 ± 50 Ma (2σ, MSWD = 0.24, n = 4), and the concordia age of the three concordant analyses is 1888.4 ± 8.8 Ma (2σ, decay-constant errors included).

5.3. Geochemistry

Due to limited age control, only three samples were available for geochemical analyses and clearly only preliminary conclusions about the geochemical characteristics of the dykes can be made based on these data. Two samples from WDS09 and one sample from 16WDS02 (same dyke as 16WDS01) were analysed for major and trace elements and for Sr and Nd isotopes. Data for the samples are presented together with major and trace element geochemistry from the 1210 Ma Marnda Moorn LIP dykes because the latter are the only known tholeiitic dyke swarm within the Yilgarn Craton with detailed studies available both in geochronology and geochemistry.

5.3.1. Major and trace elements

All samples have LOI < 1.0 wt% and display low MgO (6.18–6.73 wt%), SiO_2 (50.12–50.43 wt%), relatively high iron (FeO_{tot} = 14.10–15.09 wt%),

Table 3
SHRIMP U-Pb data for baddeleyite from dyke samples WDS09, 16WDS01 and 16WDS6.

Spot	$f_{206\%}$	U ppm	Th ppm	Th/U	± %	Total $^{238}U/^{206}Pb$	± %	Total $^{207}Pb/^{206}Pb$	± %	$^{238}U/^{206}Pb^*$	± %	$^{207}Pb^*/^{206}Pb^*$	± %	$^{238}U/^{206}Pb^*$ Age (Ma) ± 1σ	$^{207}Pb^*/^{206}Pb^*$ Age (Ma) ± 1σ	Disc. %
WDS09N1.2B	0.40	206	5.0	0.024	1.0	3.15	1.2	0.1152	0.9	3.16	1.2	0.1117	1.3	1771 ± 19	1828 ± 23	+4
WDS09N5.38B-1	0.58	269	10.0	0.039	2.9	2.94	1.9	0.1213	0.8	2.96	1.9	0.1162	1.2	1877 ± 30	1899 ± 22	+1
WDS09RSB3.45B-1	0.72	449	76.0	0.174	7.3	2.80	1.5	0.1192	0.7	2.82	1.5	0.1129	1.3	1958 ± 25	1847 ± 23	−7
WDS09RSB1.54B-1	0.75	67	30.0	0.468	2.2	2.74	1.7	0.1196	1.5	2.76	1.7	0.1131	2.6	1994 ± 29	1849 ± 48	−9
16WDS6D.406B-1	0.08	247	23.5	0.098	1.0	2.9	1.7	0.118	1.4	2.9	1.7	0.117	1.5	1934 ± 29	1914 ± 28	−1
16WDS6D.406B-2	0.43	129	14.4	0.115	1.3	2.8	2.2	0.121	1.9	2.8	2.2	0.117	2.7	1944 ± 37	1915 ± 49	−2
16WDS6D.405B-1	0.67	251	23.9	0.098	3.9	3.0	1.8	0.122	1.7	3.1	1.8	0.116	2.8	1827 ± 29	1898 ± 50	+4
16WDS1C.372B-1	0.17	199	9.0	0.05	3.5	3.0	1.9	0.117	1.2	3.0	1.9	0.115	1.4	1870 ± 30	1881 ± 26	+1
16WDS1C.372B-2	0.07	181	6.0	0.03	2.7	2.9	1.9	0.116	1.4	2.9	1.9	0.115	1.5	1923 ± 32	1882 ± 27	−3
Excluded analyses																
WDS09N3.18B1	2.12	117	47.0	0.414	1.2	2.62	2.3	0.1379	1.8	2.67	2.3	0.1193	3.7	2050 ± 40	1946 ± 67	−6
WDS09N5.29B-1	1.45	131	8.0	0.064	3.8	3.06	2.6	0.1283	2.1	3.11	2.6	0.1156	3.3	1799 ± 42	1890 ± 60	+6
WDS09N3.21B-1	2.17	373	35.0	0.098	1.8	2.83	2.0	0.1386	0.7	2.90	2.0	0.1196	1.9	1912 ± 33	1950 ± 34	+2
WDS09N1.4B-1	0.53	97	8.0	0.082	1.1	2.57	1.6	0.1180	1.5	2.59	1.7	0.1134	2.3	2106 ± 30	1854 ± 42	−16
WDS09N1.3B-1	1.79	205	19.0	0.096	2.5	2.53	5.7	0.1401	1.4	2.58	5.7	0.1243	3.2	2113 ± 102	2019 ± 56	−5
WDS09RSB3.45B-2	3.08	178	73.0	0.425	4.2	2.28	3.9	0.1324	1.1	2.35	3.9	0.1057	3.8	2286 ± 75	1726 ± 70	−39
16WDS6D.401B-1	2.75	83	4.3	0.053	2.5	2.8	2.7	0.133	2.7	2.9	2.8	0.109	8.3	1937 ± 47	1779 ± 151	−10
16WDS6D.401B-2	2.15	47	5.9	0.129	2.3	2.3	5.9	0.124	3.7	2.3	6.0	0.105	10.1	2296 ± 116	1720 ± 185	−40

Notes: 1) f_{204} is the proportion of common Pb in ^{206}Pb, determined using the measured $^{204}Pb/^{206}Pb$ and a common Pb composition from the Stacey and Kramers (1975) model at the approximate age of the sample; 2) Disc. = 100(t[$^{207}Pb^*/^{206}Pb^*$] − t[$^{238}U/^{206}Pb^*$])/t[$^{207}Pb^*/^{206}Pb^*$].

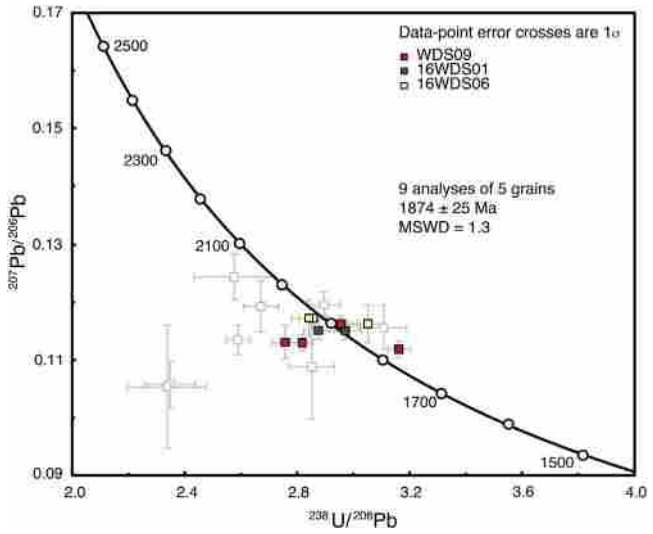

Fig. 4. Tera-Wasserburg plot of SHRIMP U-Pb baddeleyite results for samples WDS09, 16WDS01 and 16WDS06. Grey squares denote excluded data (see Section 5.1 for details).

normal to intermediate CaO (10.71–11.28 wt%) and slightly high Al_2O_3 (13.37–13.87 wt%) (Table 5). The samples have low total alkalis ($Na_2O + K_2O$ = 2.39–2.49 wt%) and high Na_2O/K_2O ratios (6.32–6.44), suggesting sodium enrichment. The Boonadgin samples are classified as sub-alkaline basalts on the TAS diagram (Fig. 6A) and belong to tholeiitic series on the AFM diagram (Fig. 6B), similar to Group 1 of the Marnda Moorn dykes (Wang et al., 2014). The chondrite normalised rare earth element (REE) distribution patterns are relatively flat (Fig. 6C) with slight enrichment of light REE (LREE), as evidenced by La_N/Yb_N = 1.48–1.57 and La_N/Sm_N = 1.18–1.26. The low Tb_N/Yb_N ratios (1.16–1.18) are similar to the average N-MORB (1.0; Sun and McDonough, 1989) and the primitive mantle-normalised trace element patterns show strong enrichment of Cs, Rb, U and Pb and a prominent negative Nb anomaly (Fig. 6D). With the exception of these fluid-mobile elements and the negative Nb anomaly, the studied samples displayed a relative flat trace element distribution patterns without significant enrichment or depletion in specific elements.

5.3.2. Nd and Sr isotopes

The same three samples were analysed for Nd and Sr isotopes (Table 5). Ratios of $^{147}Sm/^{144}Nd$ and $^{143}Nd/^{144}Nd$ are 0.1825–0.1848 and 0.512533–0.512562, respectively. The corresponding initial $\varepsilon Nd_{1.89Ga}$ values range from +1.3 to +1.6, suggesting a slightly depleted mantle component. The $^{87}Rb/^{86}Sr$ ratio ranges from 0.39999 to 0.5464, the $^{87}Sr/^{86}Sr$ ratio from 0.714588 to 0.716562, corresponding initial Sr isotopes of $(^{87}Sr/^{86}Sr)_i$ ratio varying from 0.70124 to 0.70391. The larger range of initial Sr isotope compositions is in contrast with the uniform initial Nd isotopes, and may reflect mobility of Rb. Therefore, the measured Sr isotope compositions of the studied samples may not accurately represent their primary signature.

6. Discussion

We have identified a previously unrecognized NNW-trending swarm of mafic dykes in the Yilgarn Craton, which, based on preliminary aeromagnetic interpretation, covers an area of ca. 33,000 km^2 in the southwestern part of the craton. However, until further sampling within the craton allows better delineation of the extent of the dykes, their designation as a swarm is preliminary. Emplacement of the Boonadgin dykes was synchronous with many 1890–1880 Ma LIPs worldwide, such as the Bastar-Cuddapah dykes in India (French et al., 2008; Belica et al., 2014), the Circum-Superior magmatism of the Superior Craton (Heaman et al., 1986; Halls and Heaman, 2000; Ernst and Bell, 2010), the Ghost-Mara dyke swarm of the Slave Craton (Buchan et al., 2010),

Table 4
ID-TIMS U-Pb data for baddeleyite from dyke WDS09.

Sample	wt. (µg)	U (ppm)	Pb_c (pg)	mol% Pb^*	Th/U	$^{206}Pb/^{204}Pb$	$^{207}Pb/^{206}Pb$	± (%)	$^{207}Pb/^{235}U$	± (%)	$^{206}Pb/^{238}U$	± (%)	ρ	$^{206}Pb/^{238}U$ Age (Ma)	± (Ma)	$^{207}Pb/^{206}Pb$ Age (Ma)	± (Ma)
1	0.1	38	0.8	58	0.03	98	0.11340	7.20	4.6180	8.34	0.29534	1.23	0.94	1668.1	20.5	1854.7	130.1
2	0.2	3	0.4	19	0.13	30	0.11478	7.36	5.2167	10.50	0.32962	6.28	0.72	1836.5	115.4	1876.4	132.6
3	0.1	21	0.6	56	0.01	87	0.11311	3.78	5.2972	4.46	0.33966	1.05	0.71	1885.0	19.7	1850.0	68.4
4	0.2	36	0.8	59	0.07	104	0.11710	7.75	5.5091	9.03	0.34120	1.36	0.95	1892.4	25.8	1912.5	139.1

Notes: 1) All uncertainties given at 2σ; 2) ρ = error correlation coefficient of radiogenic $^{207}Pb/^{235}U$ vs. $^{206}Pb/^{238}U$; 3) Pb_c = Total common Pb including analytical blank (0.8 ± 0.3 pg per analysis); 4) Blank composition is: $^{206}Pb/^{204}Pb$ = 18.55 ± 0.63, $^{207}Pb/^{204}Pb$ = 15.50 ± 0.55, $^{208}Pb/^{204}Pb$ = 38.07 ± 1.56 (all 2σ), and a $^{206}Pb/^{204}Pb$–$^{207}Pb/^{204}Pb$ correlation of 0.9. 5) Th/U calculated from radiogenic $^{208}Pb/^{206}Pb$ and age of 1.88 Ga; 6) Sample weights are calculated from crystal dimensions and are associated with as much as 50% uncertainty (estimated); 7) Measured isotopic ratios corrected for tracer contribution and mass fractionation (0.02 ± 0.06%/amu); 8) Ratios involving ^{206}Pb are corrected for initial disequilibrium in $^{230}Th/^{238}U$ using Th/U = 4 in the crystallization environment.

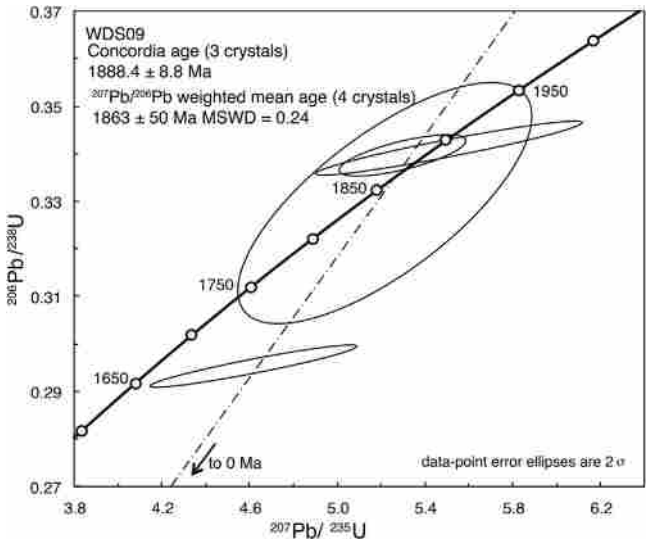

Fig. 5. Concordia plot for analysed baddeleyite ID-TIMS U-Pb results from sample WDS09.

the Uatuma dyke swarm of the Amazonian Craton (Klein et al., 2012; Antonio et al., 2017) and the Mashonaland sill province of the Zimbabwe Craton (Söderlund et al., 2010), the Soutpansperg sill province (Hanson et al., 2004) and the Black Hills dyke swarm (Olsson et al., 2016) of the Kaapvaal Craton. In the following sections, we discuss the emplacement of the dykes within the regional tectonic setting, coeval magmatism elsewhere in the region, and the implications for a recently proposed tectonic reconstruction, which raises the possibility that the dykes may be associated with the Bastar-Cuddapah LIP in India.

6.1. Coeval magmatism in Australia

No other mafic magmatism within uncertainty of the 1888 ± 9 Ma age for the Boonadgin dyke swarm is currently known in the WAC or elsewhere in Australia. However, felsic tuffs from a succession of granular iron formation (GIF) in the Frere Formation in the Earaheedy Basin have been dated at 1891 ± 8 Ma and 1885 ± 18 Ma, and linked to voluminous mantle input from an oceanic mafic source during a major global episode of mantle upwelling and crustal growth (Rasmussen et al., 2012). Evidence of synchronous magmatism elsewhere in the Capricorn Orogen is limited to a 1900 Ma zircon population peak from the Chiall Formation in the upper sequence of the Earaheedy Basin (Halilovic et al., 2004).

Ameen and Wilde (2006) reported WSW-trending mafic dykes with a zircon SHRIMP U-Pb age of 1852 ± 12 Ma from the Yalgoo greenstone belt in the Youanmi Terrane in the northwestern Yilgarn Craton (Fig. 1), ca. 360 km NNE of Perth and ca. 350 km north of sample 16WDS06. Their emplacement suggests a further episode of lithospheric extension ca. 35 Ma after the Boonadgin dykes. The WSW orientation of the Yalgoo dykes may reflect a change in the regional stress field, the influence of local crustal architecture, or a change in the position of plume centre. There is limited, but suggestive, evidence of magmatism within the Capricorn Orogen coeval with the Yalgoo dykes. The age of the Yalgoo dykes is within uncertainty of an 1842 ± 5 Ma detrital zircon population from the Leake Spring Metamorphics, a predominantly siliciclastic sequence within the northern Gascoyne Province (Sheppard et al., 2010b) and a ca. 1860 Ma detrital zircon population from turbidites in the Ashburton Basin (Sircombe, 2002).

The temporally closest mafic magmatism in the North Australian Craton (NAC) consist of the predominantly mafic volcanic rocks of the Biscay Formation in the Halls Creek Orogen in northwestern Australia, which yielded a U-Pb zircon age of 1880 ± 3 Ma (Blake et al., 1999). The Woodward Dolerite, which comprises sills intruding the succession,

Table 5
Major, trace element and isotope data for samples WDS09M, WDS09N and 16WDS02A.

	WDS09M	WDS09N	16WDS02A		WDS09M	WDS09N	16WDS02A
SiO_2	49.68	50.42	49.91	Sm (ppm)	2.43	3.13	2.90
TiO_2	1.14	1.31	1.25	Nd (ppm)	7.93	10.37	9.54
Al_2O_3	13.75	13.42	13.26	$^{143}Nd/^{144}Nd$	0.512558	0.512533	0.512562
CaO	10.65	10.71	11.19	$^{147}Sm/^{144}Nd$	0.1848	0.1825	0.1837
Fe_2O_3(tot)	14.53	15.09	14.29	$(^{143}Nd/^{144}Nd)_i$	0.510260	0.510263	0.510278
K_2O	0.32	0.34	0.32	εNd(t)	1.3	1.3	1.6
MgO	6.67	6.18	6.59	Rb (ppm)	18.13	22.04	15.39
MnO	0.23	0.24	0.23	Sr (ppm)	102.10	116.80	111.40
Na_2O	2.05	2.15	2.06	$^{87}Rb/^{86}Sr$	0.514200	0.546400	0.399900
P_2O_5	0.095	0.119	0.108	$^{87}Sr/^{86}Sr$	0.716562	0.715838	0.714588
LOI	0.69	0.03	0.54	$(^{87}Sr/^{86}Sr)_i$	0.702820	0.701240	0.703910
Total	99.81	100.01	99.75				
Mg#	51.22	48.36	51.33		BCR-2	JND-1	
Sc	45.80	46.80	47.80	$^{143}Nd/^{144}Nd$	0.512637	0.512112	
V	302.00	310.00	315.00		0.512640	0.512117	
Co	55.30	56.90	57.70		0.512623	0.512102	
Ni	87.60	121.00	87.70		0.512633		
Ga	16.40	17.40	16.60	$^{87}Sr/^{86}Sr$	0.704987		
Ge	542.00	559.00	556.00		0.705013		
Rb	17.50	22.50	18.30				
Sr	110.00	120.00	115.00				
Y	22.60	28.40	26.70				
Zr	59.00	80.50	72.40				
Nb	3.11	4.07	3.67				
Cs	0.56	1.02	0.19				
Ba	53.90	59.40	56.80				
La	4.92	6.04	5.42				
Ce	11.90	15.00	13.10				
Pr	1.75	2.20	2.00				
Nd	8.35	10.50	9.61				
Sm	2.53	3.18	2.96				
Eu	0.96	1.12	1.05				
Gd	3.27	4.09	3.80				
Tb	0.58	0.73	0.68				
Dy	3.79	4.73	4.45				
Ho	0.83	1.05	0.98				
Er	2.37	2.94	2.77				
Tm	0.35	0.45	0.42				
Yb	2.25	2.85	2.62				
Lu	0.34	0.42	0.39				
Hf	1.63	2.19	2.00				
Ta	0.21	0.28	0.25				
Pb	2.99	3.62	1.75				
Th	0.83	1.05	0.91				
U	0.30	0.38	0.30				

Notes: 1)Major elements (XRF) are given in wt% and trace elements (ICP-MS) in ppm; 2) Mg# = 100 × Mg/(Mg + Fe), Fe^{2+}/Fe_{total} = 0.85; 3) Crystallisation age t = 1890 Ma; 4) typical internal precision (2σ) is ± 0.000015 for $^{87}Sr/^{86}Sr$ and ± 0.000014 for $^{143}Nd/^{144}Nd$; 5) Recent isotope dilution analyses for USGS basalt standard BCR-2 average 6.41 ppm Sm, 28.02 ppm Nd, $^{147}Sm/^{144}Nd$ 0.1381 ± 0.0004 and $^{143}Nd/^{144}Nd$ 0.512635 ± 0.000023 (n = 6, ± 2sd); 46.5 ppm Rb, 337.6 ppm Sr, $^{87}Rb/^{86}Sr$ 0.3982 ± 0.0010, $^{87}Sr/^{86}Sr$ 0.704987 ± 0.000015 (n = 1, ± 2se). These results are consistent with TIMS and MC-ICPMS reference values. ε_{Nd} values are calculated relative to a modern chondritic mantle (CHUR) with $^{147}Sm/^{144}Nd$ = 0.1960 and $^{143}Nd/^{144}Nd$ = 0.512632 (Bouvier et al., 2008). Age-corrected initial ε_{Nd} and $^{87}Sr/^{86}Sr$ have propagated uncertainties of ± 0.5 units and ≤ ± 0.00010 (assuming an age uncertainty of ± 5 Ma), respectively. Decay constants are ^{87}Rb 1.395E^{-11}/yr and ^{147}Sm 6.54E^{-12}/yr.

has maximum and minimum ages, respectively, of ca. 1847 Ma and 1808 Ma (Blake et al., 1997) and its emplacement age is thus closer to the Yalgoo dykes. However, the Halls Creek bimodal volcanism has been associated with convergence of two cratons unrelated to the West Australian Craton, and pre-dates amalgamation of the West Australian Craton with other cratons (Bagas, 2004; Cawood and Korsch, 2008).

6.2. Tectonic and magmatic events in the WAC at ca. 1890 Ma

The Boonadgin dyke swarm was emplaced into the western margin of the WAC, about 60 million years after the WAC was assembled along the Capricorn Orogen during the Glenburgh Orogeny at 2005–1950 Ma (Sheppard et al., 2004, 2010a; Johnson et al., 2011). Following amalgamation of the WAC, the Capricorn Orogen was the site of episodic intracontinental reworking and reactivation for more than one billion years (Cawood and Tyler, 2004b; Sheppard et al., 2010a; Johnson et al., 2011). At the time the Boonadgin dykes were emplaced, the WAC was under a period of tectonic quiescence. The ca. 1891–1885 Ma felsic volcanic rocks in the Earaheedy Basin (Rasmussen et al., 2012) were emplaced during limited rifting and suggest that at least the eastern part of the Capricorn Orogen underwent lithospheric extension at this time (Sheppard et al., 2016).

Emplacement of the NW-trending Boonadgin dykes indicates regional SW-NE oriented lithospheric extension, which is consistent with direction of coeval extension within the NW-trending Earaheedy basin. In aeromagnetic images the dykes are linear, appear to have a single magnetic polarity and extend across the southwestern craton before being apparently truncated by the Darling Fault in the west and by the Albany-Fraser Orogen in the south. The orientation of the dykes is roughly parallel to the regional NW-SE tectonic grain imparted by terrane accretion during the Archean (Middleton et al., 1993; Wilde et al., 1996; Dentith and Featherstone, 2003) and suggests that they intruded along existing crustal weaknesses controlled by a regional stress field (Hou et al., 2010; Hou, 2012; Ju et al., 2013). A seismic

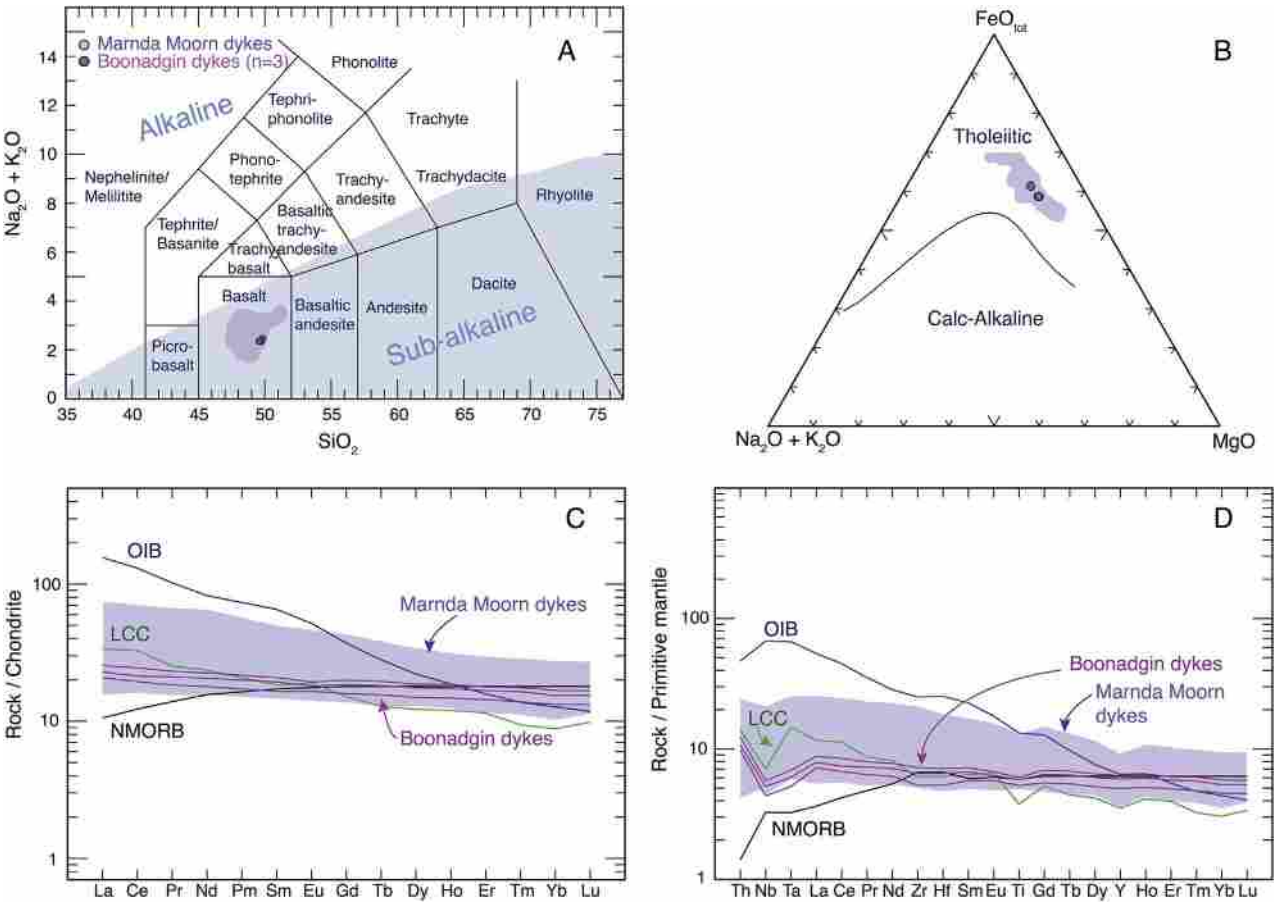

Fig. 6. (A) Total alkali-silica (TAS) plot after Le Maitre et al., 1989. Blue dots are Marnda Moorn group 1 dykes from Wang et al. (2014). (B) AFM plot after Irvine and Baragar, 1971. (C) Chondrite and (D) primitive mantle normalised multi-element plots for Boonadgin and Marnda Moorn group 1 dykes (Wang et al., 2014). LCC = lower continental crust after Rudnick and Gao (2003); OIB = ocean island basalt and NMORB = mid ocean ridge basalt after Sun and McDonough (1989). (For interpretation of the references to color in this figure legend, the reader is referred to the web version of this article.)

survey south of sample WDS09 identified a ca. 20° NE-dipping high-velocity zone, which was interpreted to represent a mafic-ultramafic body in the lower crust at ca. 30 km depth; this may be either a possible conduit for mafic magma that intruded along the suture, a zone of intrusions, or a fault-bounded terrane of possible oceanic affinity (Dentith et al., 2000; Dentith and Featherstone, 2003).

No direct Paleoproterozoic record along the western margin of Yilgarn Craton has been preserved due to younger orogenic and rifting events and it is uncertain whether it was an active plate boundary when the Boonadgin dykes were emplaced. Along the southern margin of the craton, the only known event coeval with emplacement of the Boonadgin dyke swarm could be deposition of the Stirling Range Formation in the Paleoproterozoic Barren Basin in the western Albany-Fraser Orogen. The Barren Basin comprises structural remnants of a much larger basin system deposited in an intra-continental rift or back-arc setting (Clark et al., 2000; Spaggiari et al., 2011, 2014, 2015). Formation age of the basin is unclear, but detrital zircon and monazite dating suggests that it is younger than ca. 2016 Ma and possibly formed at ca. 1895 Ma (Rasmussen and Fletcher, 2002; Rasmussen et al., 2004). Given the uncertainty of timing of early rifting in the southwest, it is difficult to link emplacement of the Boonadgin dykes with any tectonic events adjacent to the southwestern part of the craton.

6.3. Source of the Boonadgin dykes

Ratios of incompatible trace elements sensitive to source composition and partial melting effects but insensitive to crystal fractionation can be used to investigate mantle source characteristics. Zirconium can be used to evaluate mobility of major and trace elements during alteration and metamorphism (e.g., Polat et al., 2002). The Nb, Ta, Hf, Th and REE concentrations in the samples show good correlation with Zr (not shown) suggesting that these elements represent the primary composition of the dykes. The primitive mantle-normalised profile of the Boonadgin dykes (Fig. 6D; Table 5) is remarkably similar to that of the lower continental crust (LCC; Rudnick and Gao, 2003) with average ratios of Nb/La = 0.66, Th/Nb = 0.26 and Ce/Pb = 5.20 (0.63, 0.24 and 5.0, respectively for LCC). Ratios of La/Sm = 1.89 and Sm/ Nd = 0.30 are near-chondritic (1.55 and 0.33, respectively; Sun and McDonough, 1989) and close to the Marnda Moorn Group 1 dykes (ca. 1.70 and 0.28, respectively). The ratio of Nb/Ta = 14.75 is much higher than the lower crust (8.33) but close to that of depleted mantle (ca. 15; Salters and Stracke, 2004) and Marnda Moorn Group 1 dykes (ca. 15; Wang et al., 2014). The ratio of Zr/Sm = 24.36 is similar to the lower crust(ca.24)andmuchlowerthandepletedmantle(ca.29).

The similarity of the trace element compositions of the studied samples to the average value of lower continental crust suggests the possibility of lower continental crust contamination. We conducted preliminary binary mixing modelling (Depaolo, 1981) using data from the three Boonadgin dykes samples. If the primary melt had a N-MORB-like trace element composition and $\varepsilon Nd_{1.9Ga} = +8$, incorporating 20–30% of mafic lower continental crust ($\varepsilon Nd_{1.9Ga} = -10$, estimated by Nd isotope mapping of the Yilgarn (Champion, 2013) and the method proposed by Depaolo (1981) into the primary melt can produce the observed Nd isotope and trace element compositions. The lack of prominent fractionation of HREE indicates that partial melting likely occurredwithinthespinelstabilityfield(at<70kmdepth).Ifthisis

correct, the sub-continental lithospheric mantle (SCLM) beneath the margin of the Yilgarn Craton may have been largely removed or thinned. This could be attributed to lithospheric extension, consistent with basin formationalongthesouthernmarginofthecraton(Section6.2).

Another possible mechanism to produce the observed trace element compositions and slightly depleted Nd isotope signature is via melt-rock interaction with asthenospheric mantle. Because lower continental crust can founder into the convecting mantle (e.g., Gao et al., 2004), melts derived from recycled lower continental crust could interact with the ambient peridotite to form enriched pyroxenitic lithologies (Sobolev et al., 2005, 2007; Wang et al., 2014), imparting a lower continental crust signature and a slightly depleted Nd isotope signature on the resultant melts.

6.4. *Was the WAC connected to other cratons at ca. 1890 Ma?*

The position of WAC in Paleoproterozoic reconstruction models is highly debated partly due to the absence of robust paleomagnetic and high precision geochronological data for dyke swarms. For example, the WAC has been placed near India (Rogers and Santosh, 2002; Zhao et al., 2002;Mohanty,2012,2015),KaapvaalandZimbabweCratons(Zhao et al., 2002; Hou et al., 2008; Belica et al., 2014), or Siberia (Hou et al., 2008; Belica et al., 2014) in reconstructions for various Paleoproterozoic time intervals. Halls et al. (2007) used paleomagnetic data to argue that India and Australia were at high paleolatitudes but ~2000 km apart at ca. 2400–2350 Ma. Similarly, Mohanty (2012, 2015) proposed a juxtaposition of the western margin of the WAC and the eastern margin of the Bastar-Dharwar craton at ca. 2400–2300 Ma (the South India-Western Australia SIWA supercraton; Fig. 7) based on paleomagnetic data, synchronous mafic magmatism and matching dyke orientation but their relative positions by ca. 1900 Ma were unknown. Mohanty (2012, 2015) nonetheless noted that the lack of 2.0–1.8 Ga dykes in the Yilgarn Craton implies that the breakup of SIWA must have taken place during an earlier rifting event. Our discovery of the 1888 Ma Boonadgin dykes in the Yilgarn Craton makes such an early breakup unnecessary. With such a configuration at 1890 Ma, NE-SW extension and emplacement of the NW-oriented 1888 Ma Boonadgin dykes in the Yilgarn Craton is synchronous with E-W extension in- itiating the Cuddapah Basin and the associated 1890 Ma NW-oriented mafic dykes and ultramafic magmatism in the Dharwar Craton (Anand, 2003; French et al., 2008), as well as the emplacement of NW-oriented dykes in the Bastar Craton (French et al., 2008) as segments of a single radiating dyke swarm.

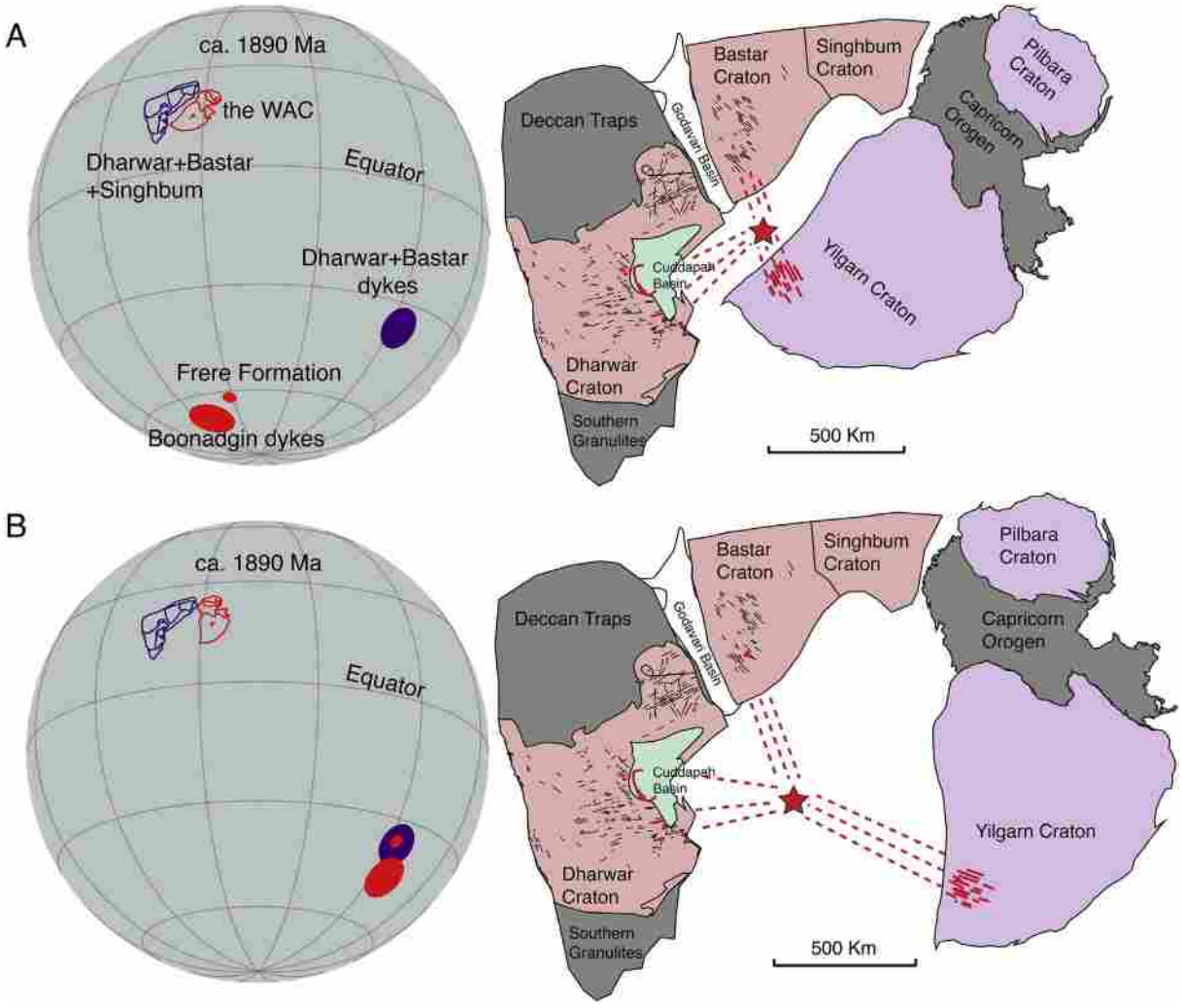

Fig. 7. Possible configurations of the WAC and Dharwar, Bastar and Singhbum cratons tested with paleomagnetic data at ca. 1890 Ma. Coeval paleopoles are plotted on the left-hand side and color coded with the respective cratons. The WAC was rotated to the Indian coordinates and more detailed reconstructions are shown on the right side. Indian dykes shown in red have been dated with U-Pb or Ar-Ar methods at 1879–1894 Ma (Chatterjee and Bhattacharji, 2001; Halls et al., 2007; French et al., 2008; Belica et al., 2014). Black undated dykes in India are modified after French et al. (2008) and Srivastava and Gautam (2015). Red star denotes possible location of a mantle plume. (A) SIWA configuration modified from ca. 2400 Ma reconstruction of Mohanty (2012); (B) Alternative configuration of Liu et al. (this issue) supported by paleomagnetic data. (For interpretation of the references to color in this figure legend, the reader is referred to the web version of this article.)

Liu et al. (this issue) obtained a high quality paleomagnetic pole from the Boonadgin dykes and used available robust paleomagnetic data to test the SIWA connection and other possible configurations. The new Boonadgin dyke pole falls close to the Frere Formation (Capricorn Orogen) pole of Williams et al. (2004), which has been considered to be 1891–1885 Ma in age (e.g., Antonio et al., 2017; Klein et al., 2016) based on zircon data from tuffs within the basal Frere Formation (Rasmussen et al., 2012). However, Williams et al. (2004) sampled the upper part of the formation, implying that the actual magnetization age for their Frere Formation pole is likely younger than 1885 Ma. Consequently, Liu et al. (this issue) suggest that the ca. 1890 Ma Boonadgin pole is coeval with the 1888–1882 Ma Dharwar-Bastar pole (Belica et al., 2014) and that the age difference between the Boonadgin and the < 1885 Ma Frere Formation poles may explain the slight difference in their positions. The Boonadgin and Dharwar-Bastar dyke poles are about 50° apart after restoration of the two continental blocks to the SIWA configuration (Fig. 7A), indicating that the SIWA fit is invalid at ca. 1890 Ma. In contrast, an alternative configuration juxtaposing the northern WAC (Pilbara) and north-eastern India (Singhbhum) is not only consistent with paleomagnetic data (Fig. 7B), but still allows the contemporaneous mafic dykes in India and the WAC to form a radiating dyke swarm. If this interpretation is correct, the 1888 Ma Boonadgin dykes in the Yilgarn Craton may be part of the Bastar-Cuddapah LIP event (French et al., 2008; Belica et al., 2014).

6.5. Could the Boonadgin dyke swarm be part of the Bastar-Cuddapah LIP?

Abundant, predominantly NW-SE to NNW-ESE oriented 1890–1880 Ma Bastar-Cuddapah LIP dykes intrude the Bastar and Dharwar cratons and form a radiating dyke swarm over at least 90,000 km^2 (Anand, 2003; Halls et al., 2007; French et al., 2008; Belica et al., 2014). In the southern Bastar Craton, BD2 dykes are oriented predominantly NW-SE to WNW-ESE (French et al., 2008). In the Dharwar craton, baddeleyite from the Pulivendla sill in the Cuddapah basin yielded an ID-TIMS $^{207}Pb/^{206}Pb$ age of 1885 ± 3 Ma (French et al., 2008) and paleomagnetic data suggest that dykes of this age also have NW-SE, E-W and NE-SW orientations depending on their location within the craton (Halls et al., 2007; Belica et al., 2014). The NW-trending dykes appear to be sub-parallel to the regional Archean structural grain in both the Bastar and Dharwar cratons, suggesting that they may have intruded along pre-existing faults and fabrics (Crookshank, 1963; Chatterjee and Bhattacharji, 2001). New SHRIMP U-Pb dating of felsic tuffs from the lowermost succession of the Cuddapah Basin, the Tadpatri Formation, yielded ca. 1864 Ma and ca. 1858 Ma, and mafic-ultramafic sills intruding this stratigraphic level (and higher) indicate that mafic magmatism continued until after ca. 1860 Ma (Sheppard et al., 2017). Dykes of < 1900 Ma age are present in both Bastar and Dharwar Cratons but their ages are currently either poorly constrained or unknown (Murthy, 1987; Mallikharjuna et al., 1995; Meert et al., 2010), making any comparison highly speculative.

Extensive coeval mafic magmatism and intracontinental rifting in the Dharwar Craton at ca. 1899–1885 Ma have been linked to a mantle plume beneath India or east of the Cuddapah Basin (Ernst and Srivastava, 2008; Belica et al., 2014; Mishra, 2015), or to passive rifting associated with a short lived global mantle upwelling (Anand, 2003; French et al., 2008). Two models have been proposed for formation of the Cuddapah Basin, one arguing for failed rifting (Chaudhuri et al., 2002) and another for full rifting and opening of an ocean basin (Kumar and Leelanandam, 2008; Kumar et al., 2010). Dasgupta et al. (2013) proposed that formation of the Cuddapah Basin at ca. 1890 Ma was associated with continental rifting between India and another craton. If this was the WAC, no evidence of equivalent basins is preserved on the western or southern margin of the Yilgarn Craton.

In contrast to the Boonadgin dykes, the Cuddapah sills are more enriched and contain a more significant melt component from the Archean lithosphere, with La_N/Sm_N ratios between 1.4 and 2.5, La_N/Yb_N ratios between 2.4 and 4.3 (1.18–1.26 and 1.48–1.57 for Boonadgin dykes, respectively) and $\varepsilon Nd_{1.89Ga}$ values between +1 and −10 (+1.3 to +1.6 for Boonadgin dykes) (Anand, 2003). Modelling of the Cuddapah sills suggests that they were produced by 15–20% partial melting of a lherzolitic mantle with a potential temperature of ~1500 °C, similar to ambient mantle of similar age and not necessarily indicative of a mantle plume (Anand, 2003). Current geochemical evidence is insufficient to determine whether the Boonadgin dykes and the Bastar-Cuddapah LIP are associated with the same mantle source.

Similar to the Yilgarn Craton where the Boonadgin and Yalgoo dykes are interpreted to be associated with discrete episodes of lithospheric extension, sills intruding the unconformity-bound sedimentary successions within the Cuddapah basin are coeval with episodes of lithospheric extension (Sheppard et al., 2017) In both cases, mafic magmatism appears to span 35–40 Ma (ca. 1890–1855 Ma) rather than comprising a short-lived event.

7. Conclusions

The Archean Yilgarn Craton in Western Australia is intruded by multiple generations of Precambrian ma^{fi}c dykes, identi^{fi}ed by previous studies. Until now, evidence for ma^{fi}c magmatism in the Yilgarn Craton at ca. 1890 Ma has been absent, surprising since ma^{fi}c magmatism of this age is found on most other Precambrian cratons worldwide. The newly named, NW-trending 1888 Ma Boonadgin dyke swarm is interpreted to extend across an area of at least 33,000 km^2 in the southwestern Yilgarn Craton. The dykes were emplaced along the southwestern margin of the Yilgarn Craton more than 50 million years after it was amalgamated with the Pilbara Craton-Glenburgh Terrane along the Capricorn Orogen to form the West Australian Craton. Intrusion of the Boonadgin dyke swarm was synchronous with minor rifting, felsic volcanism and deposition of granular iron formation in the Earaheedy Basin at the southeastern end of the Capricorn Orogen. Evidence for another pulse of ma^{fi}c magmatism at ca. 1852 Ma in the northern Yilgarn Craton was also coeval with magmatism in the Capricorn Orogen, suggesting that ma^{fi}c magmatism spanned at least 35 million years. Emplacement of the Boonadgin dyke swarm is contemporaneous with the Bastar-Cuddapah LIP and opening of the Cuddapah Basin on the eastern margin of India, and the ca. 1852 Ma Yalgoo dykes in northern Yilgarn may be coeval with ca. 1860 ma^{fi}c magmatism in the Cuddapah basin. Moreover, existing studies and recent paleomagnetic data suggest that the Yilgarn and Bastar-Cuddapah cratons were adjacent to each other at c. 1890 Ma, raising the possibility that the Boonadgin dyke swarm may be part of a wider Bastar-Cuddapah LIP. However, Meso- to Neoproterozoic orogenic activity and Phanerozoic rifting along the western margin in the Yilgarn Craton have obliterated stratigraphic successions equivalent to the Cuddapah Basin, and poor age control of extension and initial rifting in southern Yilgarn Craton do not provide reliable geological piercing points. In contrast to proposed rifting of the Yilgarn Craton from India at ca. 2300 Ma, new evidence presented in this paper suggests that the cratons may still have beenneighboursat1890Ma.

Acknowledgments

This work was funded by ARC Centre for Core to Crust Fluid Systems CoE Grant (CE110001017) and ARC Laureate Fellowship Grant (FL150100133) to Z.-X.L. JCS gratefully acknowledges support by Curtin University ORD Postgraduate Scholarship. We thank Cristina Talavera and Hao Gao for their invaluable support with SHRIMP U-Pb analyses at John de Laeter Centre, Curtin University. Roland Maas and Nenping Shen are thanked for their valuable assistance with geochemical analyses and Louise Heyworth for her help with sample preparation at UWA. We thank Larry Heaman and Michiel de Kock for their constructive and helpful reviews that greatly improved the manuscript.

References

Ameen, S.M.M., Wilde, S.A., 2006. Identification of 1.85 Ga mafic dykes in the Northern Yilgarn Craton: a relationship to the Columbia supercontinent? IAGR Annu. Conv. Int. Symp., 2006.

Anand, M., 2003. Early Proterozoic melt generation processes beneath the Intra-cratonic Cuddapah Basin, Southern India. J. Petrol. 44, 2139–2171. http://dx.doi.org/10.1093/petrology/egg073.

Anand, R.R., Paine, M., 2002. Regolith geology of the Yilgarn Craton, Western Australia: implications for exploration. Aust. J. Earth Sci. 49, 3–162.

Antonio, P.Y.J., D'Agrella-Filho, M.S., Trindade, R.I.F., Nédélec, A., de Oliveira, D.C., da Silva, F.F., Roverato, M., Lana, C., 2017. Turmoil before the boring billion: paleomagnetism of the 1880–1860 Ma Uatumã event in the Amazonian craton. Gondwana Res. 49, 106–129.

Bagas, L., 2004. Proterozoic evolution and tectonic setting of the northwest Paterson Orogen, Western Australia. Precambr. Res. 128, 475–496. http://dx.doi.org/10.1016/j.precamres.2003.09.011.

Belica, M.E., Piispa, E.J., Meert, J.G., Pesonen, L.J., Plado, J., Pandit, M.K., Kamenov, G.D., Celestino, M., 2014. Paleoproterozoic mafic dyke swarms from the Dharwar craton; paleomagnetic poles for India from 2.37 to 1.88 Ga and rethinking the Columbia supercontinent. Precambr. Res. 244, 100–122. http://dx.doi.org/10.1016/j.precamres.2013.12.005.

Blake, D.H., Tyler, I.M., Sheppard, S., 1997. Geology of the Ruby Plains 1:100 000 Sheet Area (4460), Western Australia. Australian Geological Survey Organisation.

Blake, D.H., Tyler, I.M., Griffin, T.J., Sheppard, S., Thorne, A.M., Warren, R.G., 1999. Geology of the Halls Creek 1:100 000 Sheet Area (4461), Western Australia. Aust. Geol. Surv. Organ., Canberra.

Bleeker, W., Ernst, R., 2006. Short-lived mantle generated magmatic events and their dyke swarms: the key unlocking Earth's paleogeographic record back to 2.6 Ga. In: Hanski, E.J., Mertanen, S., Rämö, O.T., Vuollo, J. (Eds.), Dyke Swarms—Time Markers of Crustal Evolution: Selected Papers of the Fifth International Dyke Conference in Finland, Rovaniemi, Finland, 31 July–3 August 2005 & Fourth International Dyke Conference, Kwazulu-Natal, South Africa 26–29 June 2001. CRC Press, London, pp. 3–26.

Boyd, D.M., Tucker, D.H., 1990. Australian magnetic dykes. In: Parker, A.J., Rickwood, P.C., Tucker, D.H. (Eds.), Mafic Dykes and Emplacement Mechanisms. A.A. Balkema, Rotterdam, pp. 391–399.

Bouvier, A., Vervoort, J.D., Patchett, P.J., 2008. The Lu–Hf and Sm–Nd isotopic composition of CHUR: constraints from unequilibrated chondrites and implications for the bulk composition of terrestrial planets. Earth Planet. Sci. Lett. 273, 48–57.

Buchan, K.L., Ernst, R.E., Hamilton, M.A., Mertanen, S., Pesonen, L.J., Elming, S.-Å., 2001. Rodinia: the evidence from integrated palaeomagnetism and U-Pb geochronology. Precambr. Res. 110, 9–32.

Buchan, K.L., Ernst, R.E., Bleeker, W., Davies, W., Villeneuve, M., van Breemen, O., Hamilton, M., Söderlund, U., 2010. Proterozoic magmatic events of the Slave craton, Wopmay orogen and environs. In: Geological Survey of Canada, Open File 5985. Geological Survey of Canada.

Campbell, I.H., McCall, G.J.H., Tyrwhitt, D.S., 1970. The Jimberlana Norite, Western Australia–a smaller analogue of the Great Dyke of Rhodesia. Geol. Mag. 107, 1–12.

Cassidy, K.F., Champion, D.C., Huston, D.L., 2005. Crustal evolution constraints on the metallogeny of the Yilgarn Craton. In: Mineral Deposit Research: Meeting the Global Challenge. Springer, pp. 901–904.

Cassidy, K.F., Champion, D.C., Krapez, B., Barley, M.E., Brown, S.J.A., Blewett, R.S., Groenewald, P., Tyler, I.M., 2006. A revised geological framework for the Yilgarn Craton, Western Australia. In: Geological Survey of Western Australia Record 8/2006. Geological Survey of Western Australia.

Cawood, P.A., Korsch, R.J., 2008. Assembling Australia: Proterozoic building of a continent. Precambr. Res. 166, 1–35. http://dx.doi.org/10.1016/j.precamres.2008.08.006.

Cawood, P.A., Tyler, I.M., 2004a. Assembling and reactivating the Proterozoic Capricorn Orogen: lithotectonic elements, orogenies, and significance. Precambr. Res. 128, 201–218. http://dx.doi.org/10.1016/j.precamres.2003.09.001.

Cawood, P.A., Tyler, I.M., 2004b. Assembling and reactivating the Proterozoic Capricorn Orogen: lithotectonic elements, orogenies, and significance. Precambr. Res. 128, 201–218.

Champion, D.C., 2013. Neodymium depleted mantle model age map of Australia: explanatory notes and user guide. Record 2013/44. Geosci. Aust. Rec. 209. http://dx.doi.org/10.11636/Record.2013.044.

Chatterjee, N., Bhattacharji, S., 2001. Petrology, geochemistry and tectonic settings of the mafic dikes and sills associated with the evolution of the Proterozoic Cuddapah Basin of south India. J. Earth Syst. Sci. 110, 433–453.

Chaudhuri, A.K., Saha, D., Deb, G.K., Deb, S.P., Mukherjee, M.K., Ghosh, G., 2002. The Purana basins of southern cratonic province of India-a case for Mesoproterozoic fossil rifts. Gondwana Res. 5, 23–33.

Claoué-Long, J.C., Hoatson, D.M., 2009. Guide to Using the Map of Australian Proterozoic Large Igneous Provinces. Geoscience, Australia.

Clark, D.J., Hensen, B.J., Kinny, P.D., 2000. Geochronological constraints for a two-stage history of the Albany – Fraser Orogen, Western Australia. Precambr. Res. 102, 155–183.

Coffin, M.F., Eldholm, O., 1994. Large igneous provinces: crustal structure, dimensions, and external consequences. Rev. Geophys. 32, 1–36. http://dx.doi.org/10.1029/93RG02508.

Compston, W., Williams, I.S., Meyer, C., 1984. U-Pb geochronology of zircons from lunar breccia 73217 using a sensitive high mass-resolution ion microprobe. J. Geophys. Res. 89, B525. http://dx.doi.org/10.1029/JB089iS02p0B525.

Condie, K.C., 2004. Supercontinents and superplume events: distinguishing signals in the geologic record. Phys. Earth Planet. Inter. 146, 319–332. http://dx.doi.org/10.1016/j.pepi.2003.04.002.

Crookshank, H., 1963. Geology of southern Bastar and Jeypore from the Bailadila range to the Eastern Ghats, 87th ed.

Dasgupta, S., Bose, S., Das, K., 2013. Tectonic evolution of the Eastern Ghats Belt, India. Precambr. Res. 227, 247–258. http://dx.doi.org/10.1016/j.precamres.2012.04.005.

Dentith, M.C., Featherstone, W.E., 2003. Controls on intra-plate seismicity in south-western Australia. Tectonophysics 376, 167–184. http://dx.doi.org/10.1016/j.tecto.2003.10.002.

Dentith, M.C., Dent, V.F., Drummond, B.J., 2000. Deep crustal structure in the south-western Yilgarn Craton, Western Australia. Technophysics 325, 227–255.

Depaolo, D.J., 1981. Trace element and isotopic effects of combined wallrock assimilation and fractional crystallization. Earth Planet. Sci. Lett. 53, 189–202.

Doehler, J.S., Heaman, L.M., 1998. 2.41 Ga U-Pb Baddeleyite ages for two gabbroic dykes from the Widgiemooltha swarm, Western Australia: a Yilgarn-Lewisian connection, in: America Annual Meeting in Toronto A.

Eggins, S.M., Woodhead, J.D., Kinsley, L.P.J., Mortimer, G.E., Sylvester, P., McCulloch, M.T., Hergt, J.M., Handler, M.R., 1997. A simple method for the precise determination of ≥40 trace elements in geological samples by ICPMS using enriched isotope internal standardisation. Chem. Geol. 134, 311–326.

Ernst, R.E., Bell, K., 2010. Large igneous provinces (LIPs) and carbonatites. Mineral. Petrol. 98, 55–76.

Ernst, R., Bleeker, W., 2010. Large igneous provinces (LIPs), giant dyke swarms, and mantle plumes: significance for breakup events within Canada and adjacent regions from 2.5 Ga to the present. Can. J. Earth Sci. 47, 695–739. http://dx.doi.org/10.1139/e10-025.

Ernst, R.E., Buchan, K.L., 1997. Giant radiating dyke swarms: their use in identifying pre-Mesozoic large igneous provinces and mantle plumes. In: Large Igneous Provinces: Continental, Oceanic, and Planetary Flood Volcanism. vol. 100. American Geophysical Union Monograph, pp. 297–333.

Ernst, R.E., Srivastava, R.K., 2008. India's place in the Proterozoic world: constraints from the Large Igneous Province (LIP) record. In: Srivastava, R.K., Sivaji, Ch., Chalapathi Rao, N.V. (Eds.), Geochemistry, Geophys. Geochronology Narosa Publ. House Pvt. Ltd, New Delhi, India, pp. 41–56.

Ernst, R.E., Head, J.W., Parfitt, E., Grosfils, E., Wilson, L., 1995. Giant radiating dyke swarms on Earth and Venus. Earth-Sci. Rev. 39, 1–58.

Ernst, R.E., Wingate, M.T.D., Buchan, K.L., Li, Z.X., 2008. Global record of 1600–700 Ma Large Igneous Provinces (LIPs): implications for the reconstruction of the proposed Nuna (Columbia) and Rodinia supercontinents. Precambr. Res. 160, 159–178. http://dx.doi.org/10.1016/j.precamres.2007.04.019.

Ernst, R., Srivastava, R., Bleeker, W., Hamilton, M., 2010. Precambrian Large Igneous Provinces (LIPs) and their dyke swarms: new insights from high-precision geochronology integrated with paleomagnetism and geochemistry. Precambr. Res. 183, 7–11.

Ernst, R.E., Bleeker, W., Söderlund, U., Kerr, A.C., 2013. Large Igneous Provinces and supercontinents: toward completing the plate tectonic revolution. Lithos 174, 1–14.

Evans, M.E., 1968. Magnetization of dikes: a study of the paleomagnetism of the Widgiemooltha dike suite, Western Australia. J. Geophys. Res. 73, 3261–3270.

Evans, T., 1999. Extent and Nature of the 1.2 Ga Wheatbelt Dyke Swarm, Yilgarn Craton, Western Australia (B.Sc. thesis). Univ. West. Aust., Perth.

French, J.E., Heaman, L.M., 2010. Precise U-Pb dating of Paleoproterozoic mafic dyke swarms of the Dharwar craton, India: implications for the existence of the Neoarchean supercraton Sclavia. Precambr. Res. 183, 416–441. http://dx.doi.org/10.1016/j.precamres.2010.05.003.

French, J.E., Heaman, L.M., Chacko, T., 2002. Feasibility of chemical U-Th-total Pb baddeleyite dating by electron microprobe. Chem. Geol. 188, 85–104. http://dx.doi.org/10.1016/S0009-2541(02)00074-8.

French, J.E., Heaman, L.M., Chacko, T., Srivastava, R.K., 2008. 1891–1883 Ma Southern Bastar-Cuddapah mafic igneous events, India: a newly recognized large igneous province. Precambr. Res. 160, 308–322. http://dx.doi.org/10.1016/j.precamres.2007.08.005.

Gao, S., Rudnick, R.L., Yuan, H.-L., Liu, X.-M., Liu, Y.-S., Xu, W.-L., Ling, W.-L., Ayers, J., Wang, X.-C., Wang, Q.-H., 2004. Recycling lower continental crust in the North China craton. Nature 432, 892–897.

Goldberg, A.S., 2010. Dyke swarms as indicators of major extensional events in the 1.9–1.2 Ga Columbia supercontinent. J. Geodyn. 50, 176–190.

Halilovic, J., Cawood, P.A., Jones, J.A., Pirajno, F., Nemchin, A.A., 2004. Provenance of the Earaheedy Basin: implications for assembly of the Western Australian Craton. Precambr. Res. 128, 343–366.

Hallberg, J.A., 1987. Postcratonization mafic and ultramafic dykes of the Yilgarn Block. Aust. J. Earth Sci. 34, 135–149. http://dx.doi.org/10.1080/08120098708729398.

Halls, H.C., Heaman, L.M., 2000. The paleomagnetic significance of new U-Pb age data from the Molson dyke swarm, Cauchon Lake area, Manitoba. Can. J. Earth Sci. 37, 957–966.

Halls, H.C., Zhang, B., 1998. Uplift structure of the southern Kapuskasing zone from 2.45 Ga dike swarm displacement. Geology 26, 67–70. http://dx.doi.org/10.1130/0091-7613(1998) 026<0067:USOTSK>2.3.CO;2.

Halls, H.C., Kumar, A., Srinivasan, R., Hamilton, M.A., 2007. Paleomagnetism and U-Pb geochronology of easterly trending dykes in the Dharwar craton, India: feldspar clouding, radiating dyke swarms and the position of India at 2.37 Ga. Precambr. Res. 155, 47–68. http://dx.doi.org/10.1016/j.precamres.2007.01.007.

Hanson, R.E., Gose, W.A., Crowley, J.L., Ramezani, J., Bowring, S.A., Bullen, D.S., Hall, R.P., Pancake, J.A., Mukwakwami, J., 2004. Paleoproterozoic intraplate magmatism and basin development on the Kaapvaal Craton: Age, paleomagnetism and geochemistry of ~1.93 to ~1.87 Ga post-Waterberg dolerites. South Afr. J. Geol. 107, 233–254.

Heaman, L.M., 2009. The application of U-Pb geochronology to mafic, ultramafic and alkaline rocks: an evaluation of three mineral standards. Chem. Geol. 261, 43–52. http://dx.doi.org/10.1016/j.chemgeo.2008.10.021.

Heaman, L.M., Machado, N., Krogh, T.E., Weber, W., 1986. Precise U-Pb zircon ages for the Molson dyke swarm and the Fox River sill: constraints for Early Proterozoic crustal evolution in northeastern Manitoba, Canada. Contrib. Miner. Petrol. 94, 82–89.

Heaman, L.M., Peck, D., Toope, K., 2009. Timing and geochemistry of 1.88 Ga Molson Igneous Events, Manitoba: insights into the formation of a craton-scale magmatic and metallogenic province. Precambr. Res. 172, 143–162.

Hoek, J.D., Seitz, H.-M., 1995. Continental mafic dyke swarms as tectonic indicators: an example from the Vestfold Hills, Antarctica. Precambr. Res. 75, 121–139.

Hou, G., 2012. Mechanism for three types of mafic dyke swarms. Geosci. Front. 3, 217–223. http://dx.doi.org/10.1016/j.gsf.2011.10.003.

Hou, G., Santosh, M., Qian, X., Lister, G.S., Li, J., 2008. Configuration of the Late Paleoproterozoic supercontinent Columbia: insights from radiating mafic dyke swarms. Gondwana Res. 14, 395–409. http://dx.doi.org/10.1016/j.gr.2008.01.010.

Hou, G., Kusky, T.M., Wang, C., Wang, Y., 2010. Mechanics of the giant radiating Mackenzie dyke swarm: a paleostress field modeling. J. Geophys. Res. Solid Earth 115. http://dx.doi.org/10.1029/2007JB005475.

Irvine, T.N.J., Baragar, W., 1971. A guide to the chemical classification of the common volcanic rocks. Can. J. Earth Sci. 8, 523–548.

Isles, D.J., Cooke, A.C., 1990. Spatial associations between post-cratonisation dykes and gold deposits in the Yilgarn Block, Western Australia. In: Parker, A.J., Rickwood, P.C., Tucker, D.H. (Eds.), Mafic Dykes and Emplacement Mechanisms. Balkema, Rotterdam, pp. 147–162.

Jaffey, A.H., Flynn, K.F., Glendenin, L.E., Bentley, W.C., Essling, A.M., 1971. Precision measurement of half-lives and specific activities of U 235 and U 238. Phys. Rev. C 4, 1889.

Johnson, S.P., Sheppard, S., Rasmussen, B., Wingate, M.T.D., Kirkland, C.L., Muhling, J.R., Fletcher, I.R., Belousova, E.A., 2011. Two collisions, two sutures: punctuated pre-1950 Ma assembly of the West Australian Craton during the Ophthalmian and Glenburgh Orogenies. Precambr. Res. 189, 239–262. http://dx.doi.org/10.1016/j.precamres.2011.07.011.

Ju, W., Hou, G., Hari, K.R., 2013. Mechanics of mafic dyke swarms in the Deccan Large Igneous Province: Palaeostress field modelling. J. Geodyn. 66, 79–91. http://dx.doi.org/10.1016/j.jog.2013.02.002.

Kamber, B.S., Greig, A., Schoenberg, R., Collerson, K.D., 2003. A refined solution to Earth's hidden niobium: implications for evolution of continental crust and mode of core formation. Precambr. Res. 126, 289–308.

Klein, E.L., Almeida, M.E., Rosa-Costa, L.T., 2012. The 1.89–1.87 Ga Uatumã Silicic Large Igneous Province, northern South America. November LIP of the Month [WWW Document]. URL http://www.largeigneousprovinces.org/12nov.

Klein, R., Pesonen, L.J., Mänttäri, I., Heinonen, J.S., 2016. A late Paleoproterozoic key pole for the Fennoscandian Shield: a paleomagnetic study of the Keuruu diabase dykes, Central Finland. Precambr. Res. 286, 379–397. http://dx.doi.org/10.1016/j.precamres.2016.10.013.

Ksienzyk, A.K., Jacobs, J., Boger, S.D., Koler, J., Sircombe, K.N., Whitehouse, M.J., 2012. U-Pb ages of metamorphic monazite and detrital zircon from the Northampton Complex: evidence of two orogenic cycles in Western Australia. Precambr. Res. 198–199, 37–50. http://dx.doi.org/10.1016/j.precamres.2011.12.011.

Kumar, K.V., Leelanandam, C., 2008. Evolution of the Eastern Ghats belt, India: a plate tectonic perspective. Geol. Soc. India 72, 720–749.

Kumar, K.V., Ernst, W.G., Leelanandam, C., Wooden, J.L., Grove, M.J., 2010. First Paleoproterozoic ophiolite from Gondwana: Geochronologic-geochemical documentation of ancient oceanic crust from Kandra, SE India. Tectonophysics 487, 22–32. http://dx.doi.org/10.1016/j.tecto.2010.03.005.

Le Maitre, R.W.B., Dudek, P., Keller, A., Lameyre, J., Le Bas, J., Sabine, M.J., Schmid, P.A., Sorensen, R., Streckeisen, H., Woolley, A., 1989. A classification of igneous rocks and glossary of terms: recommendations of the International Union of Geological Sciences, Subcommission on the Systematics of Igneous Rocks. International Union of Geological Sciences, Blackwell Scientific.

Lewis, J.D., 1994. Mafic dykes in the Williams-Wandering area, Western Australia. Geol. Surv. West Aust. Rep. 37, 37–52.

Li, Z.-X., Zhong, S., 2009. Supercontinent–superplume coupling, true polar wander and plume mobility: plate dominance in whole-mantle tectonics. Phys. Earth Planet. Inter. 176, 143–156. http://dx.doi.org/10.1016/j.pepi.2009.05.004.

Liu, Y., Li, Z.-X., Pisarevsky, S.A., Stark, J.C., 2016. Paleomagnetic investigation of mafic dykes in the southwestern Yilgarn Craton, Western Australia. In: Australian Earth Sciences Convention 2016 Abstracts. Geological Society of Australia, pp. 277.

Liu, Y., Li, Z.-X., Pisarevsky, S.A., Kirscher, U., Mitchell, R.N., Stark, J.C., 2017. Palaeomagnetism of the 1.89 Ga Boonadgin dykes of the Yilgarn Craton: possible connection with India. Precambr. Res In Review.

Ludwig, K., 2009. Squid 2.50, A User's Manual (No. 2.50.11.02.03 Rev. 03 Feb 2011). Berkeley, California, USA.

Ludwig, K.R., 2011. Isoplot/Ex, Version 4.15: A geochronological toolkit for Microsoft Excel: Geochronology Center Berkeley, v. 4.

Ludwig, K., 2012. User's Manual for Isoplot Version 3.75–4.15: A Geochronological Toolkit for Microsoft. Berkeley Geochronological Cent. Spec. Publ.

Maas, R., Kamenetsky, M.B., Sobolev, A.V., Kamenetsky, V.S., Sobolev, N.V., 2005. Sr, Nd, and Pb isotope evidence for a mantle origin of alkali chlorides and carbonates in the Udachnaya kimberlite, Siberia. Geology 33, 549–552.

Maas, R., Grew, E.S., Carson, C.J., 2015. Isotopic constraints (Pb, Rb-Sr, Sm-Nd) on the sources of early Cambrian pegmatites with Boron and Beryllium minerals in the Larsemann Hills, Prydz Bay, Antarctica. Can. Mineral. 53, 249–272.

Mallikharjuna, R.J., Bhattacharji, S., Rao, M.N., Hermes, O.D., 1995. 40Ar–39Ar ages and geochemical characteristics of dolerite dykes around the Proterozoic Cuddapah Basin, South India, in: Geological Society of India Memoir 33, pp. 307–328.

Meert, J.G., Pandit, M.K., Pradhan, V.R., Banks, J., Sirianni, R., Stroud, M., Newstead, B., Gifford, J., 2010. Precambrian crustal evolution of Peninsular India: a 3.0 billion year odyssey. J. Asian Earth Sci. 39, 483–515. http://dx.doi.org/10.1016/j.jseaes.2010.04.026.

Middleton, M.F., Wilde, S.A., Evans, B.A., Long, A., Dentith, M., 1993. A preliminary interpretation of deep seismic reflection and other geophysical data from the Darling Fault Zone, Western Australia. Explor. Geophys. 24, 711–718.

Minifie, M., Kerr, A.C., Ernst, R.E., Pearce, J.A., 2008. The origin, nature and consequences of the Circum-Superior 1880 Ma Large Igneous Province. Geochim. Cosmochim. Acta Suppl. 72, A633.

Mishra, D.C., 2015. Plume and Plate Tectonics Model for formation of some Proterozoic Basins of India along Contemporary Mobile Belts: Mahakoshal – Bijawar, Vindhyan and Cuddapah Basins. J. Geol. Soc. India 85, 525–536.

Mohanty, S., 2012. Spatio-temporal evolution of the Satpura Mountain Belt of India: a comparison with the Capricorn Orogen of Western Australia and implication for evolution of the supercontinent Columbia. Geosci. Front. 3, 241–267. http://dx.doi.org/10.1016/j.gsf.2011.10.005.

Mohanty, S., 2015. Precambrian continent assembly and dispersal events of South Indian and East Antarctic Shields. Int. Geol. Rev. 57, 1992–2027. http://dx.doi.org/10.1080/00206814.2015.1048751.

Morris, P.A., 2007. Composition of the Bunbury Basalt (BB1) and Kerba Monzogranite (KG1) geochemical reference materials, and assessing the contamination effects of mill heads, in: Geological Survey of Western Australia Record 2007/14. Geological Survey of Western Australia Record 2007/14.

Murthy, N.G.K., 1987. Mafic dyke swarms of the Indian shield. In: Mafic Dyke Swarms 34, pp. 393–400.

Myers, J.S., 1990. Pinjarra orogen. In: Geology and Mineral Resources of Western Australia. State Printing Division, pp. 264–274.

Myers, J.S., 1993. Precambrian Tectonic history of the West Australian Craton and Adjacent Orogens. Annu. Rev. Earth Planet. Sci. 21, 453–485.

Nelson, D.R., Myers, J.S., Nutman, A.P., 1995. Chronology and evolution of the Middle Proterozoic Albany-Fraser Orogen, Western Australia. Aust. J. Earth Sci. 42, 481–495. http://dx.doi.org/10.1080/08120099508728218.

Nemchin, A.A., Pidgeon, R.T., 1997. Evolution of the Darling range batholith, Yilgarn craton, western Australia: a SHRIMP zircon study. J. Petrol. 38, 625–649.

Nemchin, A.A., Pidgeon, R.T., 1998. Precise conventional and SHRIMP baddeleyite U-Pb age for the Binneringie Dyke, near Narrogin, Western Australia. Aust. J. Earth Sci. 45, 673–675.

Nemchin, A.A., Pidgeon, R.T., Wilde, S.A., 1994. Timing of Late Archaean granulite facies metamorphism in the southwestern Yilgarn Craton of Western Australia: evidence from U-Pb ages of zircons fro mafic granulites. Precambr. Res. 68, 307–321.

Olsson, J.R., Klausen, M.B., Hamilton, M.A., März, N., Söderlund, U., Roberts, R.J., 2016. Baddeleyite U-Pb ages and geochemistry of the 1875–1835 Ma Black Hills Dyke Swarm across north-eastern South Africa: part of a trans-Kalahari Craton back-arc setting? Geol. Foeren. Stockholm Foerh. 138, 183–202.

Pidgeon, R.T., Cook, T.J.F., 2003. 1214 ± 5 Ma dyke from the Darling Range, southwestern Yilgarn Craton, Western Australia. Aust. J. Earth Sci. 50, 769–773.

Pidgeon, R.T., Nemchin, A.A., 2001. 1.2 Ga Mafic dyke near York, southwestern Yilgarn Craton, Western Australia. Aust. J. Earth Sci. 48, 751–755. http://dx.doi.org/10.1046/j.1440-0952.2001.485895.x.

Pirajno, F., Hocking, R.M., Reddy, S.M., Jones, A.J., 2009. A review of the geology and geodynamic evolution of the Palaeoproterozoic Earaheedy Basin, Western Australia. Earth-Sci. Rev. 94, 39–77.

Pisarevsky, S., De Waele, B., Jones, S., Söderlund, U., Ernst, R.E., 2015. Paleomagnetism and U-Pb age of the 2.4 Ga Erayinia mafic dykes in the south-western Yilgarn, Western Australia: paleogeographic and geodynamic implications. Precambr. Res. 259, 222–231. http://dx.doi.org/10.1016/j.precamres.2014.05.023.

Polat, A., Hofmann, A.W., Rosing, M.T., 2002. Boninite-like volcanic rocks in the 3.7–3.8 Ga Isua greenstone belt, West Greenland: geochemical evidence for intra-oceanic subduction zone processes in the early earth. Chem. Geol. 184, 231–254. http://dx.doi.org/10.1016/S0009-2541(01)00363-1.

Prokoph, A., Ernst, R.E., Buchan, K.L., 2004. Time-series analysis of Large Igneous Provinces: 3500 Ma to Present. J. Geol. 112, 1–22. http://dx.doi.org/10.1086/379689.

Qiu, Y., McNaughton, N.J., Groves, D.I., Dunphy, J.M., 1999. First record of 1.2 Ga quartz dioritic magmatism in the Archaean Yilgarn Craton, Western Australia, and its significance. Aust. J. Earth Sci. 46, 421–428. http://dx.doi.org/10.1046/j.1440-0952.1999.00715.x.

Rasmussen, B., Fletcher, I.R., 2002. Indirect dating of mafic intrusions by SHRIMP U-Pb analysis of monazite in contact metamorphosed shale: an example from the Palaeoproterozoic Capricorn Orogen, Western Australia. Earth Planet. Sci. Lett. 197, 287–299. http://dx.doi.org/10.1016/S0012-821X(02)00501-0.

Rasmussen, B., Fletcher, I.R., 2010. Dating sedimentary rocks using in situ U-Pb geochronology of syneruptive zircon in ash-fall tuff & lt 1 mm thick. Geology 38, 299–302. http://dx.doi.org/10.1130/G30567.1.

Rasmussen, B., Fletcher, I.R., Bengtson, S., McNaughton, N.J., 2004. SHRIMP U-Pb dating of diagenetic xenotime in the Stirling Range Formation, Western Australia: 1.8 billion year minimum age for the Stirling biota. Precambr. Res. 133, 329–337. http://dx.doi.org/10.1016/j.precamres.2004.05.008.

Rasmussen, B., Fletcher, I.R., Bekker, A., Muhling, J.R., Gregory, C.J., Thorne, A.M., 2012. Deposition of 1.88-billion-year-old iron formations as a consequence of rapid crustal growth. Nature 484, 498–501.

Rogers, J.J.W., Santosh, M., 2002. Configuration of Columbia, a mesoproterozoic supercontinent. Gondwana Res. 5, 5–22. http://dx.doi.org/10.1016/s1342-937x(05)

70883-2.
Rudnick, R.L., Gao, S., 2003. Composition of the continental crust, in: Holland, H.D., Turekian, K.K. (Eds.), The Crust, Vol. 3. Treatise on Geochemistry. pp. 1–64.
Salters, V.J.M., Stracke, A., 2004. Composition of the depleted mantle. Geochem. Geophys. Geosyst. 5, Q05B07. http://dx.doi.org/10.1029/2003GC000597.
Sheppard, S., Occhipinti, S.A., Tyler, I.M., 2004. A 2005–1970 Ma Andean-type batholith in the southern Gascoyne Complex, Western Australia. Precambr. Res. 128, 257–277. http://dx.doi.org/10.1016/j.precamres.2003.09.003.
Sheppard, S., Bodorkos, S., Johnson, S.P., Wingate, M.T.D., Kirkland, C.L., 2010a. The Paleoproterozoic Capricorn Orogeny: intracontinental reworking not continent-continent collision. In: Geological Survey of Western Australia Report 108. Geological Survey of Western Australia.
Sheppard, S., Johnson, S.P., Wingate, M.T.D., Kirkland, C.L., Pirajno, F., 2010b. Explanatory Notes for the Gascoyne Province. Geol. Surv. West. Aust., pp. 336.
Sheppard, S., Fletcher, I.R., Rasmussen, B., Zi, J.-W., Muhling, J.R., Occhipinti, S.A., Wingate, M.T.D., Johnson, S.P., 2016. A new Paleoproterozoic tectonic history of the eastern Capricorn Orogen, Western Australia, revealed by U-Pb zircon dating of micro-tuffs. Precambr. Res. 286, 1–19. http://dx.doi.org/10.1016/j.precamres.2016.09.026.
Sheppard, S., Rasmussen, B., Zi, J.-W., Soma, V.S., Sarma, S., Mohan, M.R., Krapez, B., Wilde, S.A., McNaughton, N.J., 2017. Sedimentation and mafic magmatism in the Paleoproterozoic Cuddapah Basin, India, as a consequence of lithospheric extension. Gondwana Res. 48, 153–163. http://dx.doi.org/10.1016/j.gr.2017.04.024.
Sircombe, K.N., 2002. Reconnaissance detrital zircon geochronology provenance of the Palaeoproterozoic Ashburton Formation: implications for Pilbara and Yilgarn amalgamation. In: Australian Geological Convention Adelaide South Australia. Geological Society of Australia.
Sobolev, A.V., Hofmann, A.W., Sobolev, S.V., Nikogosian, I.K., 2005. An olivine-free mantle source of Hawaiian shield basalts. Nature 434, 590–597.
Sobolev, A.V., Hofmann, A.W., Kuzmin, D.V., Yaxley, G.M., Arndt, N.T., Chung, S.-L., Danyushevsky, L.V., Elliott, T., Frey, F.A., Garcia, M.O., Gurenko, A.A., Kamenetsky, V.S., Kerr, A.C., Krivolutskaya, N.A., Matvienkov, V.V., Nikogosian, I.K., Rocholl, A., Sigurdsson, I.A., Sushchevskaya, N.M., Teklay, M., 2007. The amount of recycled crust in sources of mantle-derived melts. Science (80-) 316, 412–417.
Söderlund, U., Johansson, L., 2002. A simple way to extract baddeleyite (ZrO_2). Geochem. Geophys. Geosyst. 3. http://dx.doi.org/10.1029/2001GC000212.
Söderlund, U., Hofmann, A., Klausen, M.B., Olsson, J.R., Ernst, R.E., Persson, P.O., 2010. Towards a complete magmatic barcode for the Zimbabwe craton: Baddeleyite U-Pb dating of regional dolerite dyke swarms and sill complexes. Precambr. Res. 183, 388–398. http://dx.doi.org/10.1016/j.precamres.2009.11.001.
Sofoulis, J., 1965. Explanatory Notes on the Widgiemooltha 1: 250,000 Geological Sheet Western Australia. Geological Survey of Western Australia.
Spaggiari, C. V, Bodorkos, S., Barquero-Molina, M., Tyler, I.M., Wingate, M.T.D., 2009. Interpreted Bedrock Geology of the South Yilgarn and of the South Yilgarn and Central Albany-Fraser Orogen, Western Australia, Record 2009/10.
Spaggiari, C.V., Kirkland, C.L., Pawley, M.J., Smithies, R.H., Wingate, M.T.D., Doyle, M.G., Blenkinsop, T.G., Clark, C., Oorschot, C.W., Fox, L.J., 2011. The Geology of the east Albany-Fraser Orogen—A Field Guide. Geol. Surv. West Aust. Rec. 2011/23 23, 97.
Spaggiari, C.V., Kirkland, C.L., Smithies, R.H., Wingate, M.T.D., 2014. Tectonic Links between Proterozoic Sedimentary Cycles, Basin Formation and Magmatism in the Albany-Fraser Orogen, Western Australia. Geological Survey of Western Australia.
Spaggiari, C.V., Kirkland, C.L., Smithies, H.R., Wingate, M.T.D., Belousova, E.A., 2015. Transformation of an Archean craton margin during Proterozoic basin formation and magmatism: the Albany-Fraser Orogen, Western Australia. Precambr. Res. 266, 440–466. http://dx.doi.org/10.1016/j.precamres.2015.05.036.
Srivastava, R.K., Gautam, G.C., 2015. Geochemistry and petrogenesis of Paleo – Mesoproterozoic mafic dyke swarms from northern Bastar craton, central India: geodynamic implications in reference to Columbia supercontinent. Gondwana Res. 28, 1061–1078.
Stacey, J.S.T., Kramers, JD, 1975. Approximation of terrestrial lead isotope evolution by a two-stage model. Earth Planet. Sci. Lett. 26, 207–221.
Stern, R.A., 2001. A New Isotopic and Trace-Element Standard for the Ion Microprobe: Preliminary Thermal Ionization Mass Spectrometry U-Pb and Electron-Microprobe Data, Geological Survey of Canada Current Research 2001-F. Geological Survey of Canada.
Stern, R.A., Bodorkos, S., Kamo, S.L., Hickman, A.H., Corfu, F., 2009. Measurement of SIMS instrumental mass fractionation of Pb isotopes during zircon dating. Geostand. Geoanal. Res. 33, 145–168. http://dx.doi.org/10.1111/j.1751-908X.2009.00023.x.
Sun, S., McDonough, W.F., 1989. Chemical and isotopic systematics of oceanic basalts: implications for mantle composition and processes. Geol. Soc. London Spec. Publ. 42, 313–345. http://dx.doi.org/10.1144/GSL.SP.1989.042.01.19.
Tucker, D.H., Boyd, D.M., 1987. Dykes of Australia detected by airborne magnetic surveys. Mafic Dyke Swarms. Geol. Assoc. Canada Spec. Pap. 34, 163–172.
Wang, X.-C., Li, Z.-X., Li, J., Pisarevsky, S.A., Wingate, M.T.D., 2014. Genesis of the 1.21 Ga Marnda Moorn large igneous province by plume–lithosphere interaction. Precambr. Res. 241, 85–103. http://dx.doi.org/10.1016/j.precamres.2013.11.008.
Wilde, S., 1999. Evolution of the Western Margin of Australia during the Rodinian and Gondwanan Supercontinent Cycles. Gondwana Res. 2, 481–499. http://dx.doi.org/10.1016/S1342-937X(05)70287-2.
Wilde, S.A., Middleton, M.F., Evans, B.J., 1996. Terrane accretion in the southwestern Yilgarn Craton: evidence from a deep seismic crustal profile. Precambr. Res. 78, 179–196.
Williams, G.E., Schmidt, P.W., Clark, D.A., 2004. Palaeomagnetism of iron-formation from the late Palaeoproterozoic Frere Formation, Earaheedy Basin, Western Australia: palaeogeographic and tectonic implications. Precambr. Res. 128, 367–383. http://dx.doi.org/10.1016/j.precamres.2003.09.008.
Wingate, M.T.D., 1999. Ion microprobe baddeleyite and zircon ages for Late Archaean mafic dykes of the Pilbara Craton, Western Australia. Aust. J. Earth Sci. 46, 493–500.
Wingate, M.T.D., 2007. Proterozoic mafic dykes in the Yilgarn Craton, in: Proceedings of Geoconferences (WA) Inc., Kalgoorlie 2007 Conference, Kalgoorlie, Western Australia, pp. 80–84.
Wingate, M.T.D., 2017. Mafic dyke swarms and large igneous provinces in Western Australia get a digital makeover. In: Geological Survey of Western Australia Record 2017/2. Geological Survey of Western Australia, pp. 4–8.
Wingate, M.T.D., Pidgeon, R.T., 2005. The Marnda Moorn LIP, a late Mesoproterozoic large igneous province in the Yilgarn craton, Western Australia. July 2005 LIP of the month [WWW Document]. URL http://www.largeigneousprovinces.org/05jul.
Wingate, M.T.D., Campbell, I.H., Compston, W., Gibson, G.M., 1998. Ion microprobe U-Pb ages for Neoproterozoic basaltic magmatism in south-central Australia and implications for the breakup of Rodinia. Precambr. Res. 87, 135–159. http://dx.doi.org/10.1016/S0301-9268(97)00072-7.
Wingate, M.T.D., Campbell, I.H., Harris, L.B., 2000. SHRIMP baddeleyite age for the Fraser dyke swarm, southeast Yilgarn Craton, Western Australia. Aust. J. Earth Sci. 47, 309–313.
Wingate, M.T.D., Pisarevsky, S.A., Evans, D.A.D., 2002. Rodinia connections between Australia and Laurentia: no SWEAT, no AUSWUS? Terra Nova 14, 121–128.
Wingate, M.T.D., Pirajno, F., Morris, P.A., 2004. Warakurna large igneous province: a new Mesoproterozoic large igneous province in west-central Australia. Geology 32, 105–108.
Zhao, G., Cawood, P.A., Wilde, S.A., Sun, M., 2002. Review of global 2.1–1.8 Ga orogens: implications for a pre-Rodinia supercontinent. Earth-Sci. Rev. 59, 125–162.